ROCK AND AGE RELATIONSHIPS WITHIN THE TALKEETNA FOREARC SUBDUCTION COMPLEX IN THE NELCHINA AREA, SOUTHERN ALASKA

By

John D. Barefoot, B.S.

A Thesis Submitted in Partial Fulfillment of the Requirements

for the Degree of

Master of Science

in

Geology

University of Alaska Fairbanks

December 2018

APPROVED:

Elisabeth Nadin, Committee Chair
Rainer Newberry, Committee Member
Mary Keskinen, Committee Member
Paul McCarthy, Chair
Department of Geosciences
Leah Berman, Dean
College of Natural Science and Mathematics
Michael Castellini, Dean
UAF Graduate School

Abstract

Subduction-zone processes are challenging to study because of the rarity of good exposures and the complexity of rock relationships within accretionary prisms. In south-central Alaska, a remarkably well-preserved exposure of subduction-related outcrops is located at the foot of Nelchina Glacier. Here, the crystalline basement of the Talkeetna volcanic arc is in contact with the mélange of its associated accretionary complex along the Border Ranges fault. A new zircon U-Pb age of an amphibolite from the Talkeetna arc mid-crustal basement just north of the fault is 188.9 ± 2.2 Ma, coincident with previously published dates from the mafic section of the arc. A new amphibole $^{40}Ar/^{39}Ar$ age from the same outcrop yields a plateau age of 182.6 ± 1.3 Ma, reflecting cooling/exhumation of this part of the arc. The mélange south of the arc and the Border Ranges fault, known as the McHugh Complex, comprises sheared metasedimentary rocks, metavolcanic rocks, and chert, and in the Nelchina area it includes a roughly 100-m-diameter block of pillow lavas that are undeformed but altered. Detailed compositional data show that the pillow lava block formed in an intraplate setting. New whole-rock $^{40}Ar/^{39}Ar$ analyses of two pillow-lava samples yielded irregular plateaus with an approximate age of 60 Ma, which we interpret to be largely reset due to reheating. Hypabyssal dikes crosscut the mélange, as well as younger accretionary prism deposits in the area, and provide a new zircon U-Pb age of 53.0 ± 0.9 Ma, which coincides with ages of near-trench plutonism across southern Alaska. This plutonism has been ascribed to subduction of a spreading ridge that migrated eastward along the southern Alaska margin. These new ages constrain the McHugh Complex formation and subsequent hydrothermal alteration to pre-55 Ma. We suggest that the pillow lava was originally part of a Triassic (or earlier) seamount that was decapitated and incorporated into the mélange as the oceanic plate entered the subduction zone. The pillow lava subsequently

underwent extensive hydrothermal alteration that almost completely reset its age during the ridge subduction event. We further posit that the Talkeetna volcanic arc and its associated accretionary prism sediments were in their current configuration during the ca. 55 Ma plutonism that was common throughout southern Alaska.

Table of Contents

List of Figures

Page

List of Tables

Page

Chapter 1: Introduction

Accretionary prisms associated with volcanic arcs are important for understanding the growth and accretion of continental crust at convergent margins. The inboard mélange of accretionary prisms records both the sedimentation and tectonic history of subduction, uplift, and post-accretion deformation (Festa et al. 2010, Festa et al. 2012). Mélange assemblages include a complex sedimentation sequence that results from imbrication of seafloor sediment as it is scraped off of the down-going plate or from mass wasting of the wedge (Festa et al. 2010). However, information can be difficult to extract from these complex rock units. The Franciscan complex in California is perhaps the most well-studied accretionary complex in the world, as it has been mapped and analyzed for well over 100 years (Lawson 1895; Wakabayashi 2015), but is still not completely understood. The Falls Lake mélange in central North Carolina is part of an accretionary complex that was deposited in the Cambrian, then subsequently overprinted during the Taconic and Alleghenian orogenies (Horton et al. 1986). This mélange was only described relatively recently, illustrating the difficulty of even recognizing accretionary prisms, especially after they have experienced such complex tectonic histories.

At the terminus of Nelchina Glacier in southern Alaska, Talkeetna arc basement is in contact with its associated accretionary prism along the Border Ranges fault (BRF; Figure 1.1). Here, recent glacial retreat has revealed new exposures of mélange. In this 0.5×2 km area, the basement of the Jurassic Talkeetna arc, its associated accretionary prism, and the megathrust along which the prism was accreted are all exposed. This area presents a unique opportunity to place the newly exposed mélange exposures within a regional framework using petrographic and geochemical analyses, constrain the timing of arc and mélange accretion and deformation using geochronology, and determine the probable origins of blocks within the mélange.

To that end, this study had three main goals:

1) Map the area at the base of Nelchina Glacier at a scale of 1:10,000 in order to place analyses into their geological and geographical context.
2) Characterize the units within the mélange using observations from outcrop, hand specimen, and thin section descriptions, as well as compositional data.
3) Constrain the timing of accretion and deformation of the mélange using geochronology of the arc basement, basalts within the mélange, and undeformed dikes that cross-cut the mélange.

To accomplish the above objectives, I utilized a variety of methods. These methods are explained in more detail in chapter 2, unless otherwise specified. Mapping was accomplished on foot with the aid of GPS at a scale of 1:10,000. Representative samples that were taken for the following analyses are listed in Table 1.1. In order to characterize blocks within the mélange, as well as rocks associated with the Talkeetna volcanic arc basement, I described outcrops, hand specimens, and thin sections of the samples. Mineralogical determinations from thin section were confirmed or clarified by detailed X-ray diffractometry (XRD). I performed X-ray fluorescence (XRF) on igneous samples within the mélange and the arc to measure major and minor element compositions of whole rocks. The same samples were sent to Washington State University Peter Hooper GeoAnalytical Lab for trace- and rare-earth element analysis using inductively coupled plasma mass spectrometry (ICP-MS). Combined, the compositional data were used to classify each igneous rock and determine its tectonic environment of formation. Zircon U-Pb isotopic ages of a sample from the Talkeetna arc basement and a sample from dikes cross-cutting the field area were sent to the University of British Columbia. A third sample from a pillow-lava block within the mélange was sent to the University of New Brunswick for zircon U-Pb dating. At each

university, laser ablation (LA) ICP-MS was used to determine isotopic ratios. All measurements and calculations associated with zircon U-Pb dating are presented in Table A.1, and in Figures 6 and A.1. Finally, four samples were sent to the University of Manitoba to determine $^{40}Ar/^{39}Ar$ isotopic ages. The data for these analyses are summarized in tables A.2 and A.3, and in Figures 7 and 12.

Chapter 1 of this thesis introduces the study, as well as an overview of mélange and the geologic background of southern Alaska. Chapter 2 is a manuscript submitted to *Canadian Journal of Earth Sciences*, presenting results of the three main goals of the project listed above. It presents detailed petrographic, geochemical, and geochronological studies of bedrock from Talkeetna arc basement, new exposures of the Nelchina area mélange, and dikes that crosscut the area. Chapter 3 presents my concluding remarks, as well as ideas for future work that I think should be pursued in this complex field area.

Mélange

The term "mélange" has been used in the literature since 1919 to refer to complexly disrupted and deformed "mixtures" of rock (Festa et al. 2010). Historically, the term has been descriptive rather than genetic, and has been used for broken formations and olistostromes of many different origins (Festa et al. 2010; Festa et al. 2012). Recently, there has been some effort to standardize the way in which mélanges are described and to define the differences between the origins of mélanges because this is significant for understanding the modes of deposition and deformation within subduction complexes (Cowan 1985; Festa et al. 2012, Wakabayashi 2015). In 1985, Cowan classified mélanges in the North American Cordillera based on structural and lithologic characteristics (Cowan 1985). In contrast, Festa et al. (2010) classified mélanges based

on their tectonic origin. Regardless of the classification, at its most basic a mélange is a complex mixture of different rock types, usually with scale-independent block-in-matrix fabric.

Composition and size of blocks included in the mélange can vary significantly depending on the origin of the mélange. The term 'exotic blocks' is used for blocks within mélange that are of higher metamorphic grade than the mélange matrix, and also for rocks that are not part of the original formation, such as a blueschist block in a shale matrix (Wakabayashi 2015). The presence or absence of exotic blocks can therefore help determine the nature of the mélange. Tectonic mélanges are made up of tectonically disrupted ocean plate stratigraphy, and all parts of it are usually metamorphosed to the same grade and include no exotic blocks (Festa et al. 2010; Wakabayashi 2015). Sedimentary mélanges are disrupted sequences resulting from sedimentary processes, such as gravitational sliding, and include exotic blocks (Festa et al. 2010; Wakabayashi 2015).

In southern Alaska, the mélange associated with the Jurassic Talkeetna volcanic arc is known as the McHugh Complex, first described by Clark (1973). The McHugh Complex is a Type II mélange, which is a "progressively disrupted sequence of mudstone, tuff, chert, and sandstone" (Cowan 1985). According to Cowan (1985), both Type I and II mélanges are deposited by gravitational mass wasting, usually in a slope environment, resulting in the creation of olistostromes (Cowan 1985). Festa et al. (2010) classify the McHugh Complex as a broken formation, or tectonic mélange. They also suggest that mélange types I, II, and III of Cowan (1985) are progressively more disrupted stages of tectonic mélange at the same tectonic setting (Festa et al. 2010). The McHugh Complex is a tectonic mélange because it contains no exotic blocks and is progressively disrupted ocean plate stratigraphy. A detailed description of the blocks within the mélange at the base of Nelchina Glacier can be found in Chapter 2.

Geologic Background

Southern Alaska terranes

The southern Alaska margin is made up of two composite allochthonous terranes that accreted throughout the Mesozoic and Cenozoic eras. These are the Wrangellia and Chugach-Prince William composite terranes (Figure 1.1; Plafker et al. 1994). The Wrangellia composite terrane comprises the Peninsular, Wrangellia, and Alexander terranes. Whereas the composite terrane accreted to North America in the Late Jurassic to Early Cretaceous (Trop and Ridgway 2007), it is likely that the individual terranes formed as one landmass or were accreted into one composite terrane before docking with the continent (Plafker et al. 1989). The Peninsular terrane makes up the majority of southwestern and south-central Alaska and is primarily made up of the Talkeetna arc and its overlying sedimentary sequences (DeBari and Coleman 1989; Rioux et al. 2007). This ocean island arc was active from ca. 202 to 153 Ma (Rioux et al. 2007).

The Chugach-Prince William terrane is the exposed accretionary prism of the Jurassic Talkeetna volcanic arc (Figure 1.1). The Border Ranges fault (BRF) is the subduction megathrust along which the Chugach terrane was accreted in the Late Jurassic and throughout the Cretaceous (e.g. Mackevett and Plafker 1974; Plafker et al. 1994; Pavlis and Roeske 2007; Amato et al. 2013). Paleogene reactivation of the fault is responsible for up to 130 km of offset (Pavlis and Roeske 2007). Rather than being a single fault strand, it is thought to comprise several anastomosing faults in a zone 5–20 km wide, prompting Pavlis and Roeske (2007) to call it the Border Ranges fault system.

The Chugach terrane represents the older portion of the subduction accretionary complex and began accreting to the southern margin of Alaska in the Late Jurassic; the Prince William terrane represents the portion that began accreting in the Paleocene and continued until the

Eocene (Amato and Pavlis 2010; Amato et al. 2013; Garver and Davidson 2015). The Chugach terrane is made up of an inboard mélange unit, the McHugh Complex, and the outboard coherent turbidite deposits of the Valdez Group (Figure 1.2; e.g. Plafker et al. 1994; Burns et al. 1991; Amato and Pavlis 2010). Volumetrically, an unnamed Late Triassic to Early Jurassic blueschist-greenschist unit makes up about 1% of the Chugach terrane, the McHugh Complex is about 10%, and the rest is made up of the Valdez Group flysch (Roeske et al. 1989; Plafker et al. 1994).

The McHugh Complex

The McHugh Complex can be further subdivided into different assemblages. Clark (1973) recognized two different assemblages within the McHugh Complex: a metavolcanic sequence and a metaclastic sequence. The metavolcanic sequence comprises argillite, chert, basalt, and rare limestone. The metaclastic sequence comprises greywacke and conglomerate. Both sequences have been metamorphosed to prehnite-pumpellyite facies, and in some locations up to greenschist facies (Burns et al. 1991; Bradley et al. 1993). Amato et al. (2013) took this idea further, identifying three distinct sequences in the McHugh Complex: the Late Triassic to Early Jurassic greenschist-blueschist unit, the Potter Creek metavolcanic assemblage, and the McHugh Creek metaclastic assemblage. Studies of detrital zircons show that the source rocks for the Potter Creek assemblage are likely the Talkeetna arc of the Peninsular terrane and the Late Jurassic to Early Cretaceous Chitina arc of the Wrangellia terrane (Figure 1.1; Amato and Pavlis 2010; Amato et al. 2013). Source rocks for the younger (metaclastic) McHugh Creek assemblage and the Valdez Group likely originated from the Coast Orogen of British Columbia (Amato and Pavlis, 2010; Amato et al. 2013).

Outboard of the McHugh Complex is the Valdez Group. This immense package of coherent turbidites is in contact with the McHugh Complex on its northern edge along the Eagle River fault (Figure 1.2; Burns et al. 1991; Pavlis and Roeske 2007). It is in contact with outboard turbidite sediments of the Cenozoic Prince William terrane along the Contact fault (Figure 1.2; Plafker et al. 1994). Detrital zircon studies of the Valdez Group show that it has a maximum depositional age of 89 Ma and was being deposited until at least 72 Ma (Amato and Pavlis 2010; Amato et al. 2013).

Southern Alaska Near-Trench Magmatism

The Chugach-Prince William composite terrane has been intruded by Paleocene to early Eocene tonalite to granite composition dikes and sills (Barker et al. 1992; Bradley et al. 2000; Lytwyn et al. 2000). Exposed from Sanak Island off of the coast of the Alaska Peninsula to Baranof Island in southeastern Alaska, these near-trench intrusions are known as the Sanak-Baranof belt (after Hudson et al. 1979) and have been attributed to trench-ridge-trench triple junction subduction that migrated eastward across the southern Alaska margin in Paleocene to Eocene time (Bradley et al. 1993; Bradley et al. 2000; Bradley et al. 2003). Two plate tectonic configuration models have been put forward to explain near-trench magmatism in southern Alaska: Kula-Farallon ridge subduction and Kula-Resurrection ridge subduction (e.g. Bradley et al. 2003; Cowen 2003; Haeussler et al. 2003; Davidson and Garver 2017). The source of the debate between these two models is the placement of the triple junction and whether the Chugach-Prince William composite terrane was deposited in place, or transported from the south (Figure 1.3; Bradley et al. 2003; Davidson and Garver 2017). The first model requires only two plates whose existence has been widely accepted: the Kula and Farallon plates. In this model, the

Chugach-Prince William composite terrane was deposited off of the west coast of North America and was transported north to Alaska on the subducting Kula plate. As it was being transported, it passed over the Kula-Farallon ridge, located around the same latitude as Vancouver Island, British Columbia is today. The interaction of the trench with the overlying sediment emplaced plutons into the composite terrane, explaining the progressively younger ages from west to east in the Sanak-Baranof belt, as well as similarly aged plutons on Vancouver Island (Bradley et al. 2003, Haeussler et al. 2003, Davidson and Garver 2017). The other model depends on both the Kula and Farallon plates, but introduces a new plate: the Resurrection plate (Bradley et al. 2003; Haeussler et al. 2003). The Resurrection plate is named after the Resurrection ophiolite, which would have been a part of the plate, and allows for the Chugach-Prince William composite terrane to have formed in place (Bradley et al. 2003; Haeussler et al. 2003). The evidence of its existence has been subducted, but the Kula-Resurrection ridge, along with the Resurrection-Farallon ridge, would also explain how near-trench plutonism arose. Included in this model are two triple junctions: one in southern Alaska, and one off of the west coast of North America near Vancouver Island. Both are subducting underneath North America, but the southern triple junction is stationary, while the northern triple junction sweeps from west to east across the southern Alaska margin as the Resurrection plate subducts, creating a slab window that causes intrusions into the overlying sediment (Bradley et al. 2003; Haeussler et al. 2003). Both of these models adequately explain the Sanak-Baranof belt, but debate between them is ongoing.

References

Amato, J.M., and Pavlis, T.L. 2010. Detrital zircon ages from the Chugach terrane, southern Alaska, reveal multiple episodes of accretion and erosion in a subduction complex. Geology, **38**: 459–462. doi:10.1130/G30719.1.

Amato, J.M., Pavlis, T.L., Clift, P.D., Kochelek, E.J., Hecker, J.P., Worthman, C.M., and Day, E.M. 2013. Architecture of the Chugach accretionary complex as revealed by detrital zircon ages and lithologic variations: Evidence for Mesozoic subduction erosion in south-central Alaska. Bulletin of the Geological Society of America, **125**: 1891–1911. doi:10.1130/B30818.1.

Barker, F., Farmer, G.L., Ayuso, R.A., Plafker, G., and Lull, J.S. 1992. The 50 Ma granodiorite of the eastern Gulf of Alaska: Melting in an accretionary prism in the forearc. Journal of Geophysical Research. **97**: 6757-6778.

Bradley, D.C., Haeussler, P.J., and Kusky, T.M. 1993. Timing of early Tertiary ridge subduction in southern Alaska. U.S. Geological Survey Bulletin 2068: 163-177.

Bradley, D.C., Parrish, R., Clendenen, W., Lux, D., Layer, P., Heizler, M., and Donley, D.T. 2000. New geochronological evidence for the timing of early Tertiary ridge subduction in southern Alaska. US Geological Survey Professional Paper 1615: 5–21.

Bradley, D.C., Kusky, T.M., Haeussler, P., Goldfarb, R., Miller, M., Dumoulin, J., Nelson, S.W., and Karl, S. 2003. Geologic signature of early Tertiary ridge subduction in Alaska. Geological Society of America Special Paper 371: 19-49.

Burns, L.E., Pessel, G.H., Little, T.A., Pavlis, T.L., Newberry, R.J., Winkler, G.R., and Decker, J. 1991. Geology of the northern Chugach Mountains, southcentral Alaska. Alaska Division of Geological and Geophysical Surveys Professional Report 94.

Clark, S.H.B. 1973. The McHugh Complex of south-central Alaska. U.S. Geological Survey Bulletin 1372-D.

Cowan, D.S. 1985. Structural styles in Mesozoic and Cenozoic mélanges in the western Cordillera of North America. Geological Society of America Bulletin, **96**: 451–462. doi:10.1130/0016-7606(1985)96<451:SSIMAC>2.0.CO;2.

Cowan, D.S. 2003. Revisiting the Baranof-Leech River hypothesis for early Tertiary coastwise transport of the Chugach-Prince William terrane. Earth and Planetary Science Letters, **213**: 463-475. doi:10.1016/S0012-821X(03)00300-5.

Davidson, C., and Garver, J. 2017. Age and origin of the Resurrection ophiolite and associated turbidites of the Chugach-Prince William terrane, Kenai Peninsula, Alaska. The Journal of Geology, **125**: 681-700. doi:10.1086/693926.

DeBari, S.M., and Coleman R.G. 1989. Examination of the deep levels of an island arc: Evidence from the Tonsina ultramafic-mafic assemblage, Tonsina, Alaska. Journal of Geophysical Research, **94**: 4373-4391.

Festa, A., Pini, G.A., Dilek, Y., and Codegone, G. 2010. Mélanges and mélange-forming processes: A historical overview and new concepts. International Geology Review, **52**: 1040-1105. doi:10.1080/00206810903557704.

Festa, A., Dilek, Y., Pini, G.A., Codegone, G., and Ogata, K. 2012. Mechanisms and processes of stratal disruption and mixing in the development of mélanges and broken formations: Redefining and classifying mélanges. Tectonophysics, **568-569**: 7-24. doi:10.1016/j.tecto.2012.05.21.

Garver, J.I., and Davidson, C.M. 2015. Southwestern Laurentian zircons in Upper Cretaceous flysch of the Chugach-Prince William terrane in Alaska. American Journal of Science, **315**: 537-556. doi:10.2475/06.2015.02.

Haeussler, P.J., Bradley, D.C., Wells, R.E., and Miller, M.L. 2003. Life and death of the Resurrection plate: Evidence for its existence and subduction in the northeastern Pacific in Paleocene-Eocene time. GSA Bulletin, **115**: 867-880.

Horton, J.W., Blake, D.E., Wylie, A.S., and Stoddard, E.F. 1986. Metamorphosed mélange terrane in the eastern Piedmont of North Carolina. Geology, **14**: 551–553.

Hudson, T., Plafker, G., and Peterman, Z.E. 1979. Paleogene anatexis along the Gulf of Alaska margin. Geology, **7**: 573-577.

Lawson, A.C. 1895. Sketch of the geology of the San Francisco Peninsula, California. U.S. Geological Survey. Annual Report, **15**: 399-476.

Lytwyn, J., Lockhart, S., Casey, J., and Kusky, T. 2000. Geochemistry of near-trench intrusives associated with ridge subduction, Seldovia Quadrangle, southern Alaska. Journal of Geophysical Research, **105**: 27957-27978.

Mackevett, E., and Plafker, G. 1974. The Border Ranges fault of south-central Alaska. Journal of Research of the U.S. Geological Survey, **2**: 323-329.

Pavlis, T.L., and Roeske, S.M. 2007. The Border Ranges fault system, southern Alaska. Geological Society of America Special Paper 431: 95–127. doi:10.1130/2007.2431(05).

Plafker, G., Nokleberg, W.J., and Lull, J.S. 1989. Bedrock geology and tectonic evolution of the Wrangellia, Peninsular, and Chugach terranes along the Trans-Alaska Crustal Transect in the Chugach Mountains and southern Copper River Basin, Alaska. Journal of Geophysical Research, **94**: 4255-4295.

Plafker, G., Moore, J.C., and Winkler, G.R. 1994. Geology of the southern Alaska margin. The Geology of Alaska: Geological Society of America. pp. 389–449. Available from http://www.dggs.alaska.gov/pubs/id/22261.

Rioux, M., Hacker, B., Mattinson, J., Kelemen, P., Blusztajn, J., and Gehrels, G. 2007. Magmatic development of an intra-oceanic arc: High-precision U-Pb zircon and whole-rock isotopic analyses from the accreted Talkeetna arc, south-central Alaska. Geological Society of America Bulletin, **119**: 1168–1184. doi:10.1130/B25964.1.

Roeske, S.M., Mattinson, J.M., and Armstrong, R.L. 1989. Isotopic ages of glaucophane schists on the Kodiak Islands, southern Alaska, and their implications for the Mesozoic tectonic history of the Border Ranges fault system. Geological Society of America Bulletin, **101**: 1021-1037.

Trop, J.M., and Ridgway, K.D. 2007. Mesozoic and Cenozoic tectonic growth of southern Alaska: A sedimentary basin perspective. Geological Society of America Special Paper 431: 55-94. doi:1130/2007.2431(04).

Wakabayashi, J. 2015. Anatomy of a subduction complex: architecture of the Franciscan Complex, California, at multiple length and time scales. International Geology Review, **57**: 669-746. doi:10.1080/00206814.2014.998728.

Table 1.1: Sample list showing sample locations and types of analyses performed on each sample. Thin sections were made of every sample and is not listed in the table.

Sample	Rock Type	Northing (m)	Easting (m)	Analyses*
16Ba01	coarse-grained gabbro	6841587	495427	
16Ba02	felsite dike	6839972	495488	XRF, XRD, ICP-MS, U-Pb
16Ba03	pillow trachyandesite	6840435	495669	XRF, XRD, ICP-MS, U-Pb, WR Ar/Ar
16Ba04-1	tonalite	6842547	495173	
16Ba04-2	tonalite	6842547	495173	
16Ba05	metasedimentary	6840799	495764	
16Ba06	trachybasalt	6840532	495814	XRF, XRD, ICP-MS
16Ba07	trachybasalt	6840331	495743	XRF, XRD, ICP-MS
16Ba08	carbonate	6840301	495698	
16Ba09	mudstone with tuff	6840121	495693	
16Ba10	trachybasalt	6840364	495621	XRF, XRD, ICP-MS
16Ba11	breccia	6840330	495621	
16Ba13	trachybasalt	6840446	495619	XRF, XRD, ICP-MS
16Ba14-1	felsite dike	6840778	495513	
16Ba14-2	felsite dike	6840778	495513	
16Ba15-1	sheared rock	6839715	495587	
16Ba15-2	sheared rock	6839715	495587	
16Ba16	trachybasalt	6840009	495583	XRF, XRD, ICP-MS
16Ba17-1	mudstone with tuff	6839828	495548	
16Ba17-2	mudstone with tuff	6839828	495548	
16Ba18	plagioclase-rich intrusive rock	6840259	495592	
16Ba19	fine-grained gabbro	6841035	495460	
16Ba20	tonalite	6841091	495525	
16Ba21	amphibolite	6841159	495522	XRF, XRD, ICP-MS, U-Pb, Hbl Ar/Ar
16Ba22	felsite dike	6840950	495515	
16Ba23-1	northern mesomélange	6840890	495528	
16Ba23-2	northern mesomélange	6840890	495528	
16Ba23-3	intrusive contact	6840890	495528	
16Ba24	trachybasalt	6840324	495746	
16Ba25	mudstone	6840173	495698	
16Ba26	sulfide rich rock from BRUMC	6841522	495402	
16Ba27	altered gabbro	6841530	495400	
16Ba28	coarse-grained gabbro	6842512	495198	Hbl Ar/Ar
16Ba29	coarse-grained gabbro	6842512	495198	
150715-12	pillow basalt	6840427	495672	XRF, XRD, ICP-MS, WR $^{40}Ar/^{39}Ar$

*XRF – X-ray fluorescence; XRD – X-ray diffractometry; ICP-MS – inductively coupled plasma mass spectrometry; U-Pb – laser ablation ICP-MS zircon U-Pb dating; Hbl Ar/Ar – Amphibole $^{40}Ar/^{39}Ar$; WR Ar/Ar – Whole-rock $^{40}Ar/^{39}Ar$

NOTE: XRD and XRF performed at the University of Alaska Fairbanks Advanced Instrumentation Laboratory. ICP-MS for trace- and rare-earth element composition performed at the Washington State University Peter Hooper GeoAnalytical Lab. U-Pb LA-ICP-MS zircon U-Pb dating performed at the University of British Columbia for samples 16Ba02 and 16Ba21, and at the University of New Brunswick for sample 16Ba03. All $^{40}Ar/^{39}Ar$ analyses performed at the University of Manitoba.

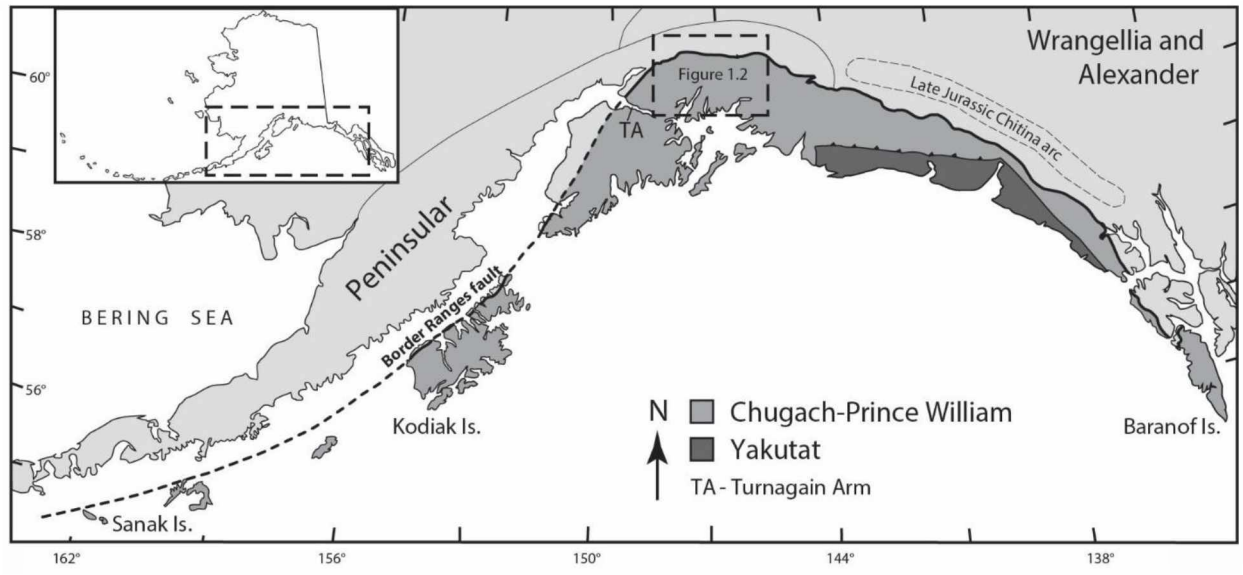

Figure 1.1: Regional map showing the general terrane configuration of southern Alaska. Dashed box is the location of Figure 1.2. The location of the Late Jurassic Chitina arc from Trop and Ridgway (2007). Modified from Garver and Davidson (2015).

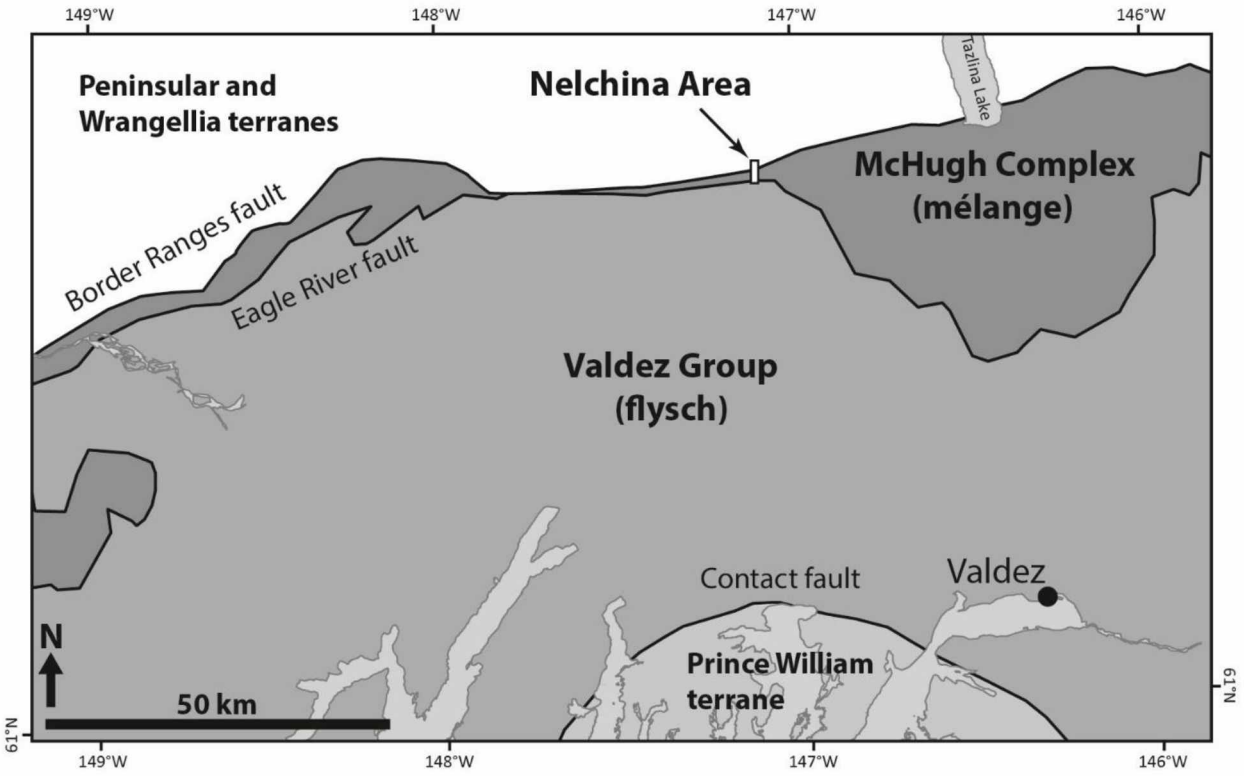

Figure 1.2: Detailed map of the Chugach-Prince William composite terrane showing the locations of its component parts. Also shown are the faults that bound each part of the composite terrane. The Border Ranges fault is the contact between the Chugach-Prince William composite terrane and the Wrangellia composite terrane. The Eagle River fault is the boundary between the mélange and flysch of the Chugach terrane. The Contact fault is the boundary between the Chugach and Prince William terranes.

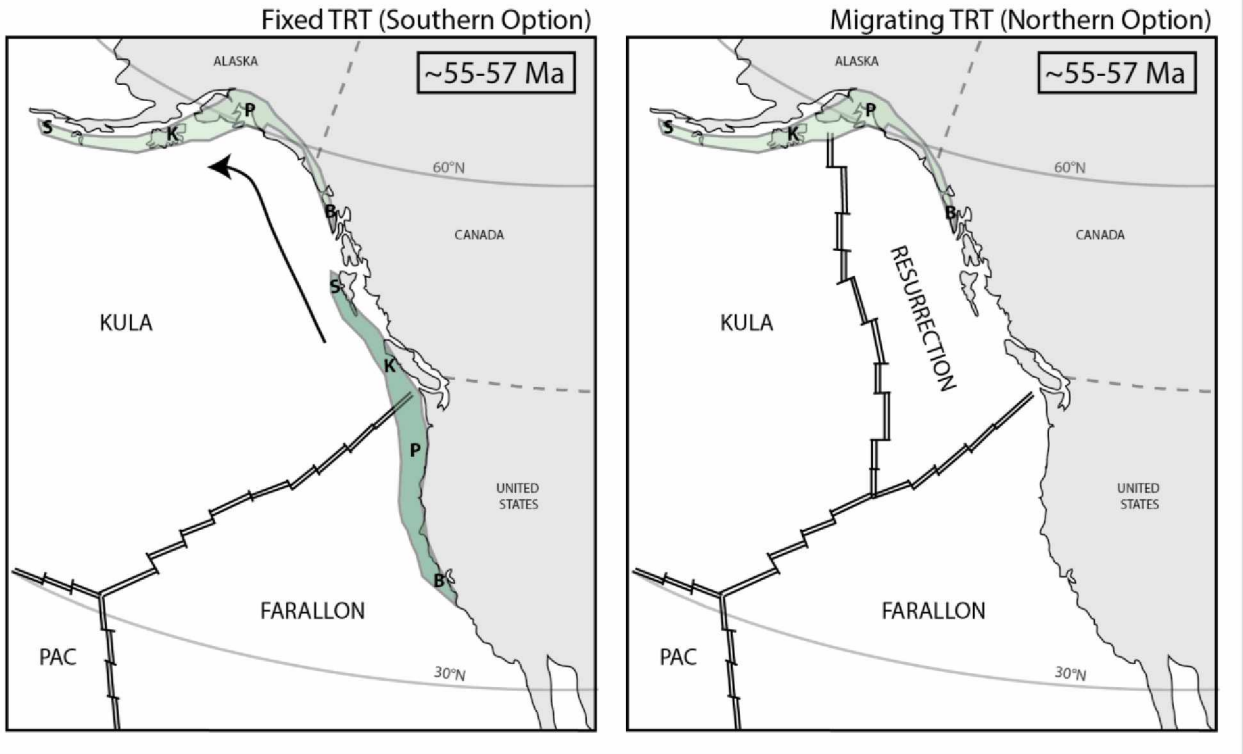

Figure 1.3: Schematic plate configuration map of the west coast of North America and southern Alaska showing two different models during Eocene time. The model on the left shows the Chugach-Prince William composite terrane being transported north to southern Alaska and passing over the subducting Kula-Farallon ridge. The model on the right shows the terrane being deposited in place, while the subducting Kula-Resurrection ridge sweeps from west to east across southern Alaska. The Resurrection-Farallon ridge remains stationary. TRT – trench-ridge-trench triple junction; S – Sanak Island; K – Kodiak Island; P – Prince William Sound; B – Baranof Island; PAC – Pacific plate. Modified from Garver and Davidson (2015).

Chapter 2: Rock and age relationships within the Talkeetna forearc subduction complex in the Nelchina area, southern Alaska

J. Barefoot[1], E.S. Nadin[1], R.J. Newberry[1], A. Camacho[2]

Corresponding author: Elisabeth Nadin (e-mail: enadin@alaska.edu).

[1] Department of Geosciences, University of Alaska Fairbanks, AK 99775, USA
[2] Department of Geological Sciences, University of Manitoba, R3T 2N2, Canada

Abstract

Subduction-zone processes are challenging to study because of the rarity of good exposures and the complexity of rock relationships within accretionary prisms. We report results of field mapping and petrographic, geochemical, and geochronological analyses of well-preserved subduction-related exposures in south-central Alaska, as well as dikes cross-cutting it, and crystalline basement juxtaposed against it. A new zircon U-Pb age from the mid-crustal basement is 188.9 ± 2.2 Ma, and its hornblende $^{40}Ar/^{39}Ar$ age is 182.6 ± 1.3 Ma, suggesting rapid cooling/exhumation of this part of the arc. The McHugh Complex mélange south of the arc in this area includes a roughly 100-m-diameter block of pillow lavas that are undeformed but pervasively hydrothermally altered. New detailed compositional data indicates the block formed in an intraplate setting. We suggest that the pillow lava was part of a seamount that was scraped off of the downgoing oceanic plate. $^{40}Ar/^{39}Ar$ analyses of these samples indicate reheating, probably by hypabyssal dikes that cross-cut the mélange and younger accretionary prism deposits (Valdez Group) in the area. A new zircon U-Pb age of 53.0 ± 0.9 Ma from the dikes coincides with ages of near-trench intrusions across southern Alaska that are associated with migration of a spreading ridge. The new ages presented here constrain McHugh Complex formation and subsequent hydrothermal alteration to pre-55 Ma. We further posit that the Talkeetna volcanic arc and its associated accretionary prism sediments were in their current configuration during the ca. 55 Ma plutonism that was common throughout southern Alaska.

I. Introduction

Arc–forearc relationships are difficult to study but are key to understanding processes that contribute to continental growth. Active margins are offshore and underwater, potentially buried by sediment. Ancient accretionary prisms are disrupted to varying degrees by substantial metamorphism and extensive large-offset faulting. The Franciscan Complex in California, for example, has been studied for >100 years (Lawson 1895; Wakabayashi 2015) due to its importance in understanding subduction-zone processes. Complexities of this type III mélange (cf. Cowan 1985) include the variability in degree of metamorphism of blocks that also have extremely variable origins and conflicting metamorphic paths, preserved within a mud matrix that is much lower grade (Cowan 1978). There is still no definitive age for subduction onset or duration (Mulcahy et al. 2018, and references therein). Similarly, the Falls Lake mélange in the Piedmont of North Carolina, also a type III mélange (cf. Cowan 1985), contains variably metamorphosed pods within a matrix of a different composition (Horton et al. 1986). This mélange was only recently recognized as such because it was overprinted several times by later orogenic events after its accretion in the Cambrian. Ancient and overprinted assemblages such as these and the McHugh mélange in southern Alaska continue to be examined for their significant insight into subduction zones.

In southern Alaska, near the retreating terminus of the Nelchina Glacier, the mid-crustal section of the Jurassic Talkeetna volcanic arc is in contact with the arc's associated accretionary mélange, the McHugh Complex (Figure 1; Pessel et al. 1981; Burns et al. 1991; Wilson et al. 2015). The contact between them is the Border Ranges fault (BRF; Figure 1), a major fault that is considered the subduction megathrust responsible for arc accretion (Plafker et al. 1994) and is heavily overprinted by Late Cretaceous to Early Paleogene strike-slip faulting (Pavlis and

Roeske 2007). In the Nelchina area, the following constituents are well exposed within a 0.5 x 2 km area that we mapped (Figure 2): the mélange of the accretionary complex; the contact between the forearc and the arc; and the mid-crustal gabbroic section of the arc (Burns et al. 1991; Burns 1996).

Bedrock near the Nelchina Glacier was previously mapped in detail with the aim of deciphering the petrologic relations of the well-exposed Talkeetna arc mid-crustal section (Burns 1985, 1996). Reconnaissance mapping south of the arc exposures, including the metasedimentary mélange sequence, was published in 1981 (Pessel et al. 1981). Glacial retreat since these maps were published has exposed large tracts of previously unmapped bedrock, including a block of pillow lava within the metasedimentary unit ~1 km south of the arc, and an intensely cataclastized zone within the accretionary complex (Yakimova and Nadin 2017). The recently exposed bedrock presents an opportunity to better characterize the accretionary prism and its relation to the juxtaposed arc section, thereby gaining further insight into the timing and nature of accretion, subduction, uplift, and subsequent deformation history of southern Alaska.

In order to determine the relationships between arc and forearc across the boundary, this paper presents the results of mapping and new geochemical and geochronological analyses of arc and associated mélange units. Our new 1:10,000-scale map of the area provides context for the analytical work, which reveals that both mid-ocean ridge basalt (MORB) and within-plate basalt (WPB) were caught in the accretionary prism. Whole-rock and amphibole $^{40}Ar/^{39}Ar$ and zircon U-Pb dates constrain the emplacement and alteration ages of Talkeetna arc basement and igneous rocks within the mélange, and a new U-Pb zircon date on a hypabyssal felsic dike that crosscuts the mélange constrains the end of BRF-related deformation. Our new analyses and mapping provide the framework for interpreting the effects of a ~200m by 250m seamount entering the

subduction zone, and how widespread near-trench plutonism across southern Alaska related to ridge subduction may have driven the pervasive hydrothermal alteration in the area.

II. Geologic Background

The southern margin of Alaska is primarily defined by two distinct composite terranes—the Wrangellia and the Chugach–Prince William composite terranes (e.g., Pavlis 1982; Bradley et al. 1993). The Wrangellia composite terrane comprises the Peninsular, Alexander, and Wrangellia terranes (Plafker and Berg 1994). The Chugach–Prince William composite terrane (also known as the Southern Margin composite terrane (e.g., Plafker et al. 1994)) consists primarily of a thick package of coherent turbidites outboard of less volumetrically significant mélange and blueschist units (Plafker et al. 1994). The boundary between the Wrangellia and Chugach–Prince William terranes has been defined as the Border Ranges fault (BRF) (e.g., MacKevett and Plafker 1974; Plafker et al. 1994; Pavlis and Roeske 2007). This fault was active in the Jurassic and early Cretaceous and is credited with the accretion of the Chugach terrane to southern Alaska (MacKevett and Plafker 1974; Pavlis and Roeske 2007). Along the BRF, the Chugach terrane is juxtaposed against the Peninsular and Wrangellia terranes, which comprise mainly Triassic to Jurassic magmatic arcs (Plafker et al. 1994). One of the most recognized of these magmatic arcs is the Jurassic Talkeetna arc, which is a large constituent of the Peninsular terrane, which is in turn part of the Wrangellia composite terrane (Plafker et al. 1989, 1994; Plafker and Berg 1994).

The Talkeetna arc of southern Alaska was an oceanic island arc that was active for ca. 40 m.y.—from 207 to 167 Ma (e.g., Amato et al. 2007). The entire arc section is preserved in the Chugach Mountains, from its lower crustal roots to its surface eruptive sequence (Rioux et al.

2007). What is considered to be the mid-crustal section of the arc is exposed along the BRF from the central Chugach Mountains southwest to Kodiak Island (Burns 1985). This complex, known as the Border Ranges ultramafic and mafic complex (BRUMC), is made up of cumulate ultramafic and gabbroic rocks that were later intruded by trondhjemite dikes (Burns 1985). This complex served as the crystalline backstop for the accretionary prism during subduction south of the arc (Little and Naeser 1989; Figure 1 of Clift and Vannucchi 2004).

South of the BRUMC and the BRF, the Chugach terrane is discontinuously exposed in an arcuate fashion from Kodiak Island in the southwest to Baranof Island in southeast Alaska (Figure 1). The inboard mélange of the Chugach terrane is the McHugh Complex (Clark 1973). The mélange is made up of two primary assemblages: a metaclastic unit and a metavolcanic unit. In this study, we refer to the metavolcanic unit as the Potter Creek Assemblage and the metaclastic unit as the McHugh Creek Assemblage, after Amato et al. (2013). The Potter Creek assemblage is older and makes up the inboard exposures of the McHugh Complex. It comprises complexly deformed and intermingled chert, argillite, basalt, and metavolcanic rocks, with local limestone and pillow basalts. This part of the mélange is a type II mélange (after Cowan 1985), due to its stratal disruption and olistostromal nature (Kusky et al. 1997). The younger McHugh Creek assemblage makes up the outboard part of the complex and comprises massive greywacke and conglomerates (Clark 1973; Amato and Pavlis 2010). The McHugh Creek assemblage is well-exposed along the north side of the Turnagain Arm, south of Anchorage (Figure 1). Studies have indicated that the McHugh Complex was intermittently accreted during episodes of subduction erosion and accretion from the Late Jurassic to Late Cretaceous (e.g., Haeussler et al. 2006; Bradley et al. 2007; Amato and Pavlis 2010). Based on detrital zircon studies, the sediment sources for the Potter Creek assemblage were the Chitina arc and the Talkeetna arc, both of

which are part of the Wrangellia composite terrane (Amato and Pavlis 2010). The younger McHugh Creek assemblage was likely sourced from the Coast orogen in the late Cretaceous (Amato and Pavlis 2010).

The Eagle River fault, a thrust fault which forms the southern boundary of the McHugh Complex in the western Chugach Mountains, separates the mélange from outboard and more volumetrically significant turbidites of the Valdez Group (Burns et al. 1991; Plafker et al. 1994). This large package of flysch is coherent and relatively undeformed, but has been variably metamorphosed from zeolite to greenschist facies (Plafker et al. 1994). Detrital zircon U-Pb ages of the Valdez Group indicate that its maximum depositional age is Late Cretaceous (e.g., Amato and Pavlis 2010; Kochelek et al. 2011). The sediment source for the flysch was likely the Coast orogen of British Colombia, Canada (Amato and Pavlis 2010).

III. Methods

Mapping

A 1 km^2 area was mapped and sampled on foot at a scale of 1:10,000 (Figure 2). Location information was determined using GPS, North American Datum 1927, UTM Zone 6. Eight map units were defined based on observed structures and, when possible, mineralogy. Ages assigned to each unit were based on Burns et al. (1991), and refined by new isotopic ages (e.g. specifying Jurassic vs. Mesozoic). Six mappable faults cut the area. Paleogene units include an undeformed matrix-supported conglomerate and three undeformed cross-cutting felsic dikes. Mesozoic units consist of undifferentiated gabbro (Early Jurassic), pillow lavas, metavolcanic rocks, metasedimentary rocks, undifferentiated mélange, and deformed mélange. Thirty-five representative samples were collected of fresh bedrock. Work was concentrated in the McHugh

complex and adjacent arc section and neither mapping nor sampling extended southward into the Valdez Group flysch.

Mineralogy

Thin section examination indicated that most of the samples are altered to fine-grained, complexly-intergrown assemblages, making mineral identification challenging. Ten samples were selected for powder x-ray diffraction (XRD) analysis. The samples were milled in the Spex 8000D Mixer/Mill for three to five minutes. To get the grain size of the resultant material below five μm, samples were micronized for ten minutes. Two mL of the micronized material were analyzed on a PANalytical X'Pert MRD x-ray diffractometer, and PANalytical's HighScore software was used for spectra interpretation.

Geochemistry

Major and minor element compositions were determined using wavelength dispersive x-ray fluorescence (WD-XRF) at the UAF Advanced Instrumentation Laboratory (AIL). Samples were crushed into fragments (typically to <0.5cm), then ~10g were milled for three to five minutes in a Spex 8000D Mixer/Mill using an 8001 hardened steel vial (~1.5% Cr, 1% C, 0.4% Mn, and 0.3% Si). Between samples, the milling vials were cleaned by milling quartz for three minutes, then rinsed with isopropyl alcohol. Resultant sample powders were mixed with a binding agent (10 drops of polyvinyl alcohol) and pressed into a 34mm pellet at 20,000 PSI for five minutes. Each pellet was analyzed using a custom PANalytical ProTrace routine on the WD-XRF. In order to determine volatile content of samples, approximately one gram of milled material was put into a ceramic crucible, which was heated in a muffle furnace for two hours at 1000°C. The sample was weighed both before and after heating to determine loss on ignition.

The PANalytical ProTrace routine was calibrated using 59 standards of a wide variety of materials. These standards have well-constrained compositional data and were used to create calibration curves so that the software could calculate concentrations from counts. Standards used for each sample were as close in composition to the sample as possible. In order to test accuracy of the WD-XRF after calibration was complete, a well-categorized basalt from Brown's Hill Quarry, Alaska, was used as a working standard.

Trace and rare-earth elemental data were collected using laser ablation inductively coupled plasma mass spectrometry (LA ICP-MS) at Washington State University's Peter Hooper GeoAnalytical Lab. Their methodology is described in Knaack et al. (1994).

U-Pb Geochronology

Three samples were selected for U-Pb geochronology: a mafic phaneritic rock from the base of the exposed arc section in the study area (16Ba21), a pillow lava from within the mélange sequence (16Ba03), and a felsic dike that crosscuts the mélange (16Ba02). Zircons for U-Pb geochronology were separated at Overburden Drilling Management Limited (ODM) using electric pulse disaggregation. Samples 16Ba02 and 16Ba21 were processed first, and their separated zircons were sent to University of British Columbia Pacific Centre for Isotopic and Geochemical Research for dating by LA ICP-MS. Sample 16Ba03 was determined by XRF to have high enough Zr concentration to warrant searching for zircons. After processing by ODM, these zircons were sent to the University of New Brunswick LA ICP-MS facility. LA ICP-MS zircon U-Pb dating methodology is described in Tafti et al. (2009).

$^{40}Ar/^{39}Ar$ geochronology

Four samples were selected for $^{40}Ar/^{39}Ar$ thermochronology: the same mafic phaneritic rock for which a zircon U-Pb age was determined (16Ba21); a coarse-grained gabbro from

within the arc section (16Ba28); and two different pillow lavas (16Ba03 and 150715-12). Dates from the two arc samples came from separated hornblende, while dates from the two pillow lavas were determined from the whole rock. The $^{40}Ar/^{39}Ar$ Geochronology Lab at the University of Manitoba crushed, separated, and dated the rocks and mineral separates.

Analyses were performed using a multi-collector Thermo Fisher Scientific ARGUSVI mass spectrometer, linked to a stainless steel Thermo Fisher Scientific extraction/purification line and Photon Machines (55 W) Fusions 10.6 CO_2 laser. Argon isotopes (from mass 40 to 37) were measured using Faraday detectors with low noise 1 x 10^{12} Ω resistors and mass 36 was measured using a compact discrete dynode (CDD) detector. The sensitivity for argon measurements is ~6.312 x 10^{17} moles/fA as determined from measured aliquots of Fish Canyon sanidine (Dazé et al. 2003; Kuiper et al. 2008).

IV. Results

Map Units

Gabbro, undifferentiated (Jgu) – These exposures of the Talkeetna arc have been mapped and interpreted as belonging to the mid-crustal section of the BRUMC (Burns 1985, 1996). They lie north of the mélange that this study focuses on, and north of the mapped trace of the BRF, which is covered by alluvium and glacial debris at the arc-mélange contact in the study area (Figure 2). The most well exposed arc rocks were sampled nearest to the mélange outcrops. These were previously mapped as gabbro (Pessel et al. 1981), but thin-section analyses reveal the rock is ~80% amphibole (Figure 3). We classify it as an amphibolite based on high amphibole content and weak fabric. Just north of this outcrop, collected samples are coarse-grained gabbro (sample 16Ba28) and tonalite dikes, as interpreted through thin-section analysis.

The amphibolite unit is ~5 m across at its widest and is largely undeformed but fractured, with calcite filling the fractures. It is fine-grained and black, with a weak fabric that strikes approximately east–west. Thin section analysis reveals anhedral and mostly pristine amphibole, with minor chlorite alteration along cleavage planes and grain fractures (Figure 3). Plagioclase is pervasively altered to zoisite and white mica and makes up ~10% of the rock. It is too altered to get a reliable composition. Sparse grains of unaltered plagioclase are An_5 (secondary albite) based on the Michel-Levy method. Apatite and zircon are accessory phases, along with ilmenite mantled by titanite (Figure 3). Pyrite occurs as small disseminated grains. Amphibole composition was determined by XRD to be ferro-pargasite.

XRF and ICP-MS on sample 16Ba21 for major, minor, trace, and rare-earth elements (Table 1) are most consistent with a MORB composition. Tectonic discrimination diagrams indicate that this rock has a MORB composition (Figure 4), but with some trace and rare-earth element (REE) concentrations up to 4 times that of normal MORB (N-MORB) (Figure 5).

Sample 16Ba21 yielded 20 zircons, from which 16 ages cluster on a U-Pb concordia plot at a weighted average of 189.9 ± 2.2 Ma and MSWD of 2.5 (Figure 6). The outlying four zircon U-Pb isotopic ages from this sample are also concordant but significantly younger than the main population, at 70.5 ± 2.6 Ma, 71.3 ± 1.6 Ma, 76.9 ± 1.9 Ma, and 102.5 ± 2.5 Ma. These outlier zircons are densely zoned, unlike the clustered zircons, and their ages likely indicate Pb loss, a later stage of zircon growth, a combined crystallization age with later zircon growth, or a more complex growth history.

Single-crystal $^{40}Ar/^{39}Ar$ analyses of hornblende from samples 16Ba21 (amphibolite) and 16Ba28 (gabbro near amphibolite) yielded well-behaved age spectra. Plateau ages of 182.6 ± 1.3

Ma (MSWD = 0.24; $\%^{39}Ar$ released = 100; Figure 7) and 184.0 ± 1.3 Ma (MSWD = 0.17; $\%^{39}Ar$ released = 57.1; Figure 7), respectively, are within error of one another.

Several dikes cut the mafic exposures near the southern edge of the arc in this area. In outcrop, these are white, coarse-grained intrusive bodies up to 5m across. Thin sections reveal the dikes are made up primarily of anhedral plagioclase and quartz. Plagioclase (An_{25-35}) is partly altered to sericite. Plagioclase twin deformation and undulatory extinction in quartz indicate that the rocks have been modestly deformed. All mafic minerals in these dikes have altered to chlorite.

Metasedimentary rocks (Mzms) – Sedimentary protoliths of the Nelchina mélange in this area have been metamorphosed to greenschist facies and have a distinct east–west striking fabric that parallels the local trace of the BRF. The metamorphic rocks include black very fine-grained metasediments, white-gray chert, green tuff, and rare limestone. Precise contacts with the northernmost dike to the north and the pillow lavas to the south are concealed by glacial till, but these units are only separated by ~20 m. Disseminated sulfides—primarily pyrite and lesser chalcopyrite—are visible in outcrop. Black mudstone that weathers orange makes up most of the metasedimentary rock volume in the area, and locally includes isolated chert ribbons and green tuff layers that are 2–3cm wide. This mudstone consists primarily of very fine- to fine-grained quartz; very fine-grained calcite, mica, and graphite; and minor albite and chlorite. Joints and fractures are filled with quartz and calcite. A stretched and folded white-gray ribbon chert block, ~10 m wide, is also exposed in the area. No fossils are visible in thin section, but elsewhere in the McHugh Complex, chert bodies with radiolarians of Late Triassic, Early Jurassic, and Early Cretaceous ages are reported (Nelson et al. 1987, Bradley and Miller 2006). Permian limestones have also been reported in the McHugh near Anchorage (Bradley and Miller 2006). In outcrop

and hand specimen, tuff is recognized in the metasedimentary units as wisps and thin layers of green swirled in with the chert and black mudstone (Figure 8). In thin section, the tuffaceous material is made up of broken grains of alkali feldspar and quartz, with a matrix of chlorite that grows around broken feldspar and quartz clasts (Figure 8).

Metavolcanic rocks (Mzmv) – The second-most dominant rock type in the Nelchina mélange is metavolcanic. These are non-uniformly distributed throughout the McHugh Complex in this location, but are likely related genetically (see geochemistry section below). Just south of the large mudstone unit, an ~100 m wide block of pillow lava is preserved (Figure 2) as a less-altered "core" within an ~250 m-wide metavolcanic block. The pillow lava, like the rest of the mélange, is metamorphosed to greenschist facies. However, the pillow structures are preserved well, with individual pillows up to 1 m wide and flattened in the upper, but not in the lower, parts of the outcrop (Figure 9). The rinds of the pillows are green, while the interiors are black and less altered. Outcrop evidence of pervasive alteration throughout these rocks (and the entire McHugh Complex) includes disseminated pyrite and calcite stringers. In thin section, glass from samples 150715-12 and 16Ba03 has been heavily altered to chlorite, but plagioclase laths up to 1mm long are preserved in random orientations (Figure 9). Most plagioclase is secondary albite, but some grains have been replaced by variably sized sericite and quartz, which are sometimes intergrown with chlorite.

Away from the core of the block, pillow structures become progressively more obscure until they are entirely absent. However, geochemical data (Table 1) indicate that the remainder of the block is the same composition as the pillowed area. In sample 16Ba07, the lavas are amygdaloidal with voids filled by calcite, chlorite, and epidote (Figure 10). Small plagioclase

laths are less common here than in sample 150715-12, but still visible in thin section within a fine-grained groundmass that has been altered to a complexly intergrown mineral assemblage.

Compositional data obtained for metavolcanic rocks in the mélange are summarized in Table 1. As these rocks have been subjected to hydrothermal alteration, the classification of Winchester and Floyd (1977) was used based on immobile elements (Figure 11). Based on their classification, the metavolcanic rocks in the mélange are all trachybasalt except for 16Ba03, which is a trachyandesite. Based on various tectonic discrimination diagrams (Figure 4), the trachybasalt samples come from a within-plate setting, except for 16Ba16, which is MORB. Trace and rare-earth element spider diagrams show a distinct trend for the within-plate basalts that closely follows the trend of average ocean island basalt from Sun and McDonough (1989) (Figure 5). Sample 16Ba03 follows the same trend but is more enriched in REEs and other incompatible elements. The spider-diagram curve for sample 16Ba16 closely parallels the N-MORB trend, showing a slight enrichment in trace elements and REEs. As mentioned earlier, sample 16Ba03 had a high Zr concentration and was sent for zircon separation and U-Pb dating. The ages spanned 3.5 Ga to 5 Ma, and we place no confidence in these results.

Step-heating $^{40}Ar/^{39}Ar$ analyses on whole-rock fragments (~1mm in diameter) of samples 16Ba03 and 150715-12 yielded discordant age spectra. Step-heating analysis for sample 150715-12 yielded a saddle-shaped age spectrum. Apparent ages increase to a maximum of ca. 80.0 Ma before falling to a saddle low of 57.0 ± 0.5 Ma (MSWD = 0.72; 31.3 % ^{39}Ar released; Figure 12a). The Ca/K values are low (~1) in the low-temperature steps and increase monotonically to a maximum of ~8 in the high-temperature steps. The increase in the Ca/K values coincides with the drop in apparent ages (Figure 12a). An additional analysis, on a separate aliquot, yielded a very similar release pattern with ages in the saddle low of 61.7 ± 1.7 Ma (MSWD = 4.0; for 35.3

% ^{39}Ar released). The ages of the low-temperature steps, and the low Ca/K ratios, may reflect recoil of ^{39}Ar (mixture of fine-grained sericite and chlorite), while the ages of the higher-temperature steps may reflect a mixture of sericite and plagioclase.

The age spectrum for sample 16Ba03 rises monotonically from ca. 50 Ma to a flat segment (two steps for 22.3% ^{39}Ar released; Figure 12b) with an age of ca. 62.5 Ma. Two additional analyses, on separate aliquots, yielded very similar release patterns with ages in the flat segment, also represented by 2 steps, of 60.3 ± 4.3 Ma (for 30.7 % ^{39}Ar released) and 60.1 ± 1.7 Ma (for 23.1 % ^{39}Ar released). Surprisingly, the Ca/K values are very low (<1) and indicate that the main potassic mineral is sericite; the monotonic increase in age may reflect the size of different white-mica domains. The smaller grains (small domains) may have a lower closure temperature than the larger domains (e.g., McDougall and Harrison 1988). The maximum apparent age may be interpreted to represent the maximum age estimate for the time of initial closure of sericite (~320°C; McDougall and Harrison 1988). Alternatively, the shape of the age spectra may reflect partial argon loss during a low-temperature thermal perturbation (presented in the Discussion section).

Mesomélange (Mzm) – This unit is made of complexly intermingled Mzms and Mzmv, much like the rest of the Nelchina mélange in this location, but at a smaller scale. Blocks in this unit are generally no larger than 10 m. The boundaries between these blocks are commonly mudstone that has a fine lamination, but blocks are infrequently in direct contact. The lamination in the mudstone indicates mineral compaction and alignment and possible flow. This unit may represent progressive stratal disruption during olistostromal sliding, as suggested by Cowan (1985) for Type II mélange.

Deformed mélange (Mzdm) – In outcrop, this unit has a fabric that is subparallel to the trace of both the BRF and the Eagle River fault. The rock is friable in outcrop and hand specimen. It is most similar to Mzms, as it contains both mudstone and green tuff swirled together. In this particular unit, however, chlorite in the tuffaceous parts (identified in thin section) defines a weak foliation that is not present in Mzms. In outcrop this section of the mélange is foliated and folded, and in thin section chlorite is seen to flow around alklali feldspar and quartz clasts. The easternmost exposure of this unit in this location, along the shore of the Nelchina River, is pulverized fault rock (Yakimova and Nadin 2017). In thin section, relict quartz clasts within the fault zone are seen to be dynamically recrystallized, indicating that the fault was active from ductile into brittle conditions.

Hypabyssal ("felsite") dikes (Pgi) – Three felsic hypabyssal dikes cross-cut the mélange in the Nelchina area. They range from ~25 m to ~150 m wide (Figures 2 & 13), are undeformed but intensely altered, and have weathered to orange-pink. The southernmost of the three dikes is the most altered. The northernmost dike is the best exposed and least weathered, although it is still highly altered. Phenocrysts of plagioclase, which make up ~10% of the rock, are 3–4 mm long in a gray, aphanitic groundmass. In thin section, visible twins indicate that the plagioclase is albite, via the Michel-Levy method. These plagioclase phenocrysts have been almost fully altered to sericite and calcite. The fine-grained groundmass consists primarily of quartz, feldspar and white mica. Clusters of chlorite, white mica, and oxides are likely alteration products of previous mafic minerals. These clusters are sparse in the northernmost dike and absent from the southernmost dike. These dikes were originally classified as "felsite" (Burns et al. 1991) because they are felsic but their original compositions are impossible to determine. Although XRF analyses provide compositional data that would classify these dikes as dacite (Table 1), we return to the

original felsite nomenclature because the composition of the plagioclase is altered and the outcrop thus precludes proper classification.

The age of the southernmost of the three dikes that crosscut the Nelchina mélange in this location was determined (Figure 2). The weighted mean $^{206}U/^{238}U$ age of sample 16Ba02 based on 20 zircons is 53.04 ± 0.93 Ma with a MSWD of 0.65 (Figure 6).

Chickaloon Formation (Pgcg) – This matrix-supported conglomerate is stratigraphically above all other units in the field area and unconformably overlies Mzdm in the southern part of the map area. Clast size varies from pebble to boulder. Except to note its contact with the mélange, this unit was not mapped. Little (1988) and Little and Naeser (1989) provided a detailed description of the conglomerate in this study area.

V. Discussion

Cooling and uplift of the Talkeetna arc

This study presents the first detailed map of mélange exposures at the base of Nelchina Glacier. Glacier retreat over the past 35 years has exposed significant tracts of outcrop since the last mapping (Burns et al. 1991), and presented the opportunity to expand our understanding of the Talkeetna arc and its related accretionary prism. We present here our interpretations based on new data from these exposures.

New U-Pb zircon crystallization ages of ca. 190 Ma (Figure 6) from BRUMC exposures just north of the Border Ranges fault in the Chugach Mountains support previous studies that place the Talkeetna intraoceanic arc against North America in the Jurassic period (Trop and Ridgway 2007). Exhumation and uplift are thought to have occurred along the Border Ranges subduction megathrust (Pavlis and Roeske 2007), which was active from late Triassic to early

Cretaceous (MacKevett and Plafker 1994; Pavlis and Roeske 2007). According to our new thermochronometric results, this portion of the arc cooled from zircon crystallization temperatures near 900 °C (Dahl 1997) to hornblende Ar closure temperatures of 500°C (e.g., Harrison 1981) in ca. 7 Myrs (Figure 7). Cooling and exhumation rates are influenced by many factors, including rock thermophysical properties, possible heat production in the region, fault kinematics and geometry, topography, and the erosion history of the region (e.g., Ehlers 2005; Braun, 2005). Such an evaluation is beyond the scope of our study, which focuses mainly on the mélange, but our results are consistent with cooling ages determined by Rioux et al. (2007) and Hacker et al. (2011) for the Chugach Mountains and Alaska Peninsula. A very preliminary cooling rate of 50 °C/Myr for this section of the arc is consistent with block uplift as suggested by Little and Naesser (1989), but the early uplift and cooling history of this section of the arc has not yet been fully evaluated.

The trace-element and REE trend for the amphibolite does not indicate oceanic arc source; rather, it follows an N-MORB trend closely with Pb, P, and Ti enrichments (Figure 5). This rock is from the Talkeetna arc mid-crustal section but does not have an arc signature (Figure 4). It also lacks the Nb-Ta anomaly typical of arc rocks (e.g., Morris and Hart 1983; McCulloch and Gamble 1991; Saunders et al. 1991). The geochemical data, paired with the anomalous rock type—amphibolite within a vast stretch of gabbro—leads us to interpret sample 16Ba21 as oceanic crust that was metamorphosed to hornblende-hornfels facies by intrusion of gabbronorite dikes and sills during arc plutonism (after Burns 1996).

McHugh Complex deposition

At the waning stages of arc accretion and Talkeetna arc volcanism in the Late Jurassic to Early Cretaceous, sediment began to fill the trench with input from both the arc and the

subducting oceanic lithosphere. The subducting plate was presumably buoyant, as the McHugh Complex records both subduction accretion and erosion episodes (Amato and Pavlis 2010, Amato et al. 2013). The oceanic plate was covered in clays and chert, and studded with seamounts, some reportedly with a limestone cap (Bradley and Miller 2006) that are Permian in age, based on fossil evidence (Bradley et al. 1999; Karl et al. 2015). We suggest that in our study area, such a seamount entered the subduction zone. The seamount is preserved as a ~200 m by 250 m block of pillow lava with a well-defined within-plate origin (Figure 4) captured within mélange of the accretionary prism. Following Cloos (1993), who suggested that even small seamounts (<1–2 km tall) can have an effect on the accretionary prism, we suggest that the seamount in the Nelchina area could have impacted the subduction process in this location. This is supported by the prevalence of mesomélange outboard of the seamount, indicating disruption of the accretionary wedge during its subduction and incorporation into the accretionary prism (Cloos 1993; Dominguez et al. 2000).

The southern metavolcanic exposure has a distinctly different signature. Sample 16Ba16 is N-MORB, based on trace-element and REE discrimination diagrams (Figures 4 & 5). This particular exposure may have been oceanic crust at the trailing edge of the subducting seamount, an interpretation which is strengthened by the proximity of ribbon chert and mudstone exposures.

The exposures of McHugh Complex in the Nelchina area form an ~2 km-long strip from north to south (Figure 2). They comprise a mélange that is tectonic in origin, based on the definition of Wakabayashi (2015). Wakabayashi (2015) details a tectonic mélange as one whose block-in-matrix structure developed primarily through tectonic processes, resulting in ocean-plate stratigraphy lacking exotic blocks, and the same metamorphic grade throughout all blocks and including the matrix. In this study area, both the matrix of the Nelchina mélange and the

blocks are metamorphosed to greenschist facies and all blocks are part of ocean plate stratigraphy, thus not exotic. The "block-in-matrix" descriptor is self-similar at multiple scales, and can be applied to the matrix between the larger blocks, which is finer-grained material that surrounds larger "blocks" that are only a few mm to cm in diameter. The matrix is clay- to sand-size particles, flowing around and between these larger clasts (Figure 14). In outcrop, it resembles ductile shearing, but in thin section there is no evidence of dynamic recrystallization. The clasts that are caught in the matrix are the same types of rocks that make up the larger blocks within the Nelchina mélange.

The constituents of the Nelchina mélange match described occurrences of the McHugh Complex in southern Alaska, both west and south of the Nelchina area (e.g., Clark 1973, Plafker et al. 1994). However, the Nelchina mélange is higher grade than these exposures, which are typically prehnite-pumpellyite (e.g., Clark 1973, Kusky et al. 1997). Whereas the McHugh Complex is typically metamorphosed only to prehnite-pumpellyite facies (e.g., Clark 1973, Kusky et al. 1997), exposures of greenschist and blueschist facies rocks related to the accretionary prism were mapped on Kodiak Island (Roeske et al. 1989), in the Seldovia quadrangle of the Kenai Peninsula (Bradley et al. 1999), and rare exposures of lower-greenschist facies McHugh Complex have been recognized in the northern Chugach Mountains (Plafker et al. 1994). The Nelchina mélange is one of the much less common parts of the McHugh Complex that has been metamorphosed to greenschist facies, which indicates that this particular area was subducted more deeply before being uplifted and exhumed. An alternative is that it was overprinted by a later episode of high-temperature metamorphism.

Sedimentary blocks within this part of the McHugh Complex are made up primarily of chert and mudstone, which are frequently intermingled. These units are part of ocean floor

stratigraphy that were incorporated into the accretionary wedge and became part of the upper plate during subduction. Tuffaceous material is swirled in with the mudstone and chert, and following similar interpretations elsewhere (e.g., Amato et al. 2013), we suggest that it erupted from the Talkeetna arc and was deposited into the mélange.

Post-McHugh Complex deposition and deformation

Granitic to tonalitic intrusions are common across both the McHugh Complex and the Valdez Group in what has been named the Sanak-Baranof belt of near-trench magmatism (Bradley et al. 1993, Bradley et al. 2000). This chain of intrusions is thought to have arisen due to the subduction of a ridge that then migrated eastward during Paleocene to Eocene time (Bradley et al. 1993, Bradley et al. 2000). The intrusions are small dikes parallel or perpendicular to the regional fabric, or large intrusions (Bradley et al. 2000). In the Nelchina area, McHugh Complex rocks are intruded by ca. 54 Ma undeformed dikes (Figure 6). These felsic hypabyssal dikes match the descriptions and compositional analyses of similarly aged dikes that intrude McHugh Complex and Valdez Group rocks elsewhere in the accretionary complex (Barker et al. 1992, Bradley et al. 2000, Lytwyn et al. 2000). Their presence through Valdez and McHugh exposures indicates that Valdez Group rocks have been in place in southern Alaska since at least 55 Ma. It would be exceedingly challenging to transpose these rocks from >2000 km away, as was recently proposed (Garver and Davidson 2015; Davidson and Garver 2017), in merely 15 Myrs after they were deposited (ca. 70 Ma: Amato et al. 2010, 2013). Sustained plate rates of >13 cm/yr seem unlikely.

In addition to placing constraints on the timing of McHugh and Valdex deposition at the southern edge of Alaska, the zircon U-Pb dike age of ca. 53 Ma supports the trend of eastward-younging ages suggested by Bradley et al. (2000) for the Sanak-Baranof intrusive belt (Figure

15). It indicates that the study area underwent a high-temperature event at around this time. The $^{40}Ar/^{39}Ar$ ages indicated by the lower-temperature saddles for the pillow basalts (Figure 12) can thus be interpreted as partial resetting of the argon isotope systematics.

Pervasive hydrothermal alteration through the area is recorded by fracture fill of quartz and calcite, chlorite-albite alteration in the basalts, the ubiquitous presence of pyrite, and the 60–50 Ma reset ages of the basalt blocks within the mélange. We suggest that this thermal event was driven by the ca. 55 Ma emplacement of the dikes during an interval of high heat flow that is consistent with passage of a spreading ridge at this location (Bradley et al. 1993; Bradley et al. 2000). The currently exposed configuration places the seamount exposure between the northernmost dike, which is ~200 m wide and ~250 m away from the northern edge of the seamount, and the central dike, which is ~35 m wide and ~130 m from the southern edge of the seamount (Figure 2). It is impossible to determine the 55 Ma configuration of these dikes, which may have been connected as roof over the seamount, thereby imparting a significant thermal overprint. The mid-crustal exposures of the Talkeetna arc seem unperturbed by the intrusions: despite being also ~200 m away from the nearest dike, the hornblende $^{40}Ar/^{39}Ar$ analyses of both the amphibolite and its surrounding gabbro yielded well-defined plateau ages of ca. 185 Ma (Figure 7), close to the crystallization (U-Pb zircon) age of the amphibolite and significantly predating dike intrusion. The dikes are also completely undeformed in a region that is otherwise pervasively sheared, suggesting that deformation associated with the BRF is older than 55 Ma in this location. Prevalent fractures throughout the Nelchina mélange, including in the metavolcanics, suggest that the thermal event drove substantial fluid flow through the mélange, leading to quartz and calcite fill of the fractures.

VI. Conclusions

In the region near the Nelchina Glacier of southern Alaska, the Talkeetna arc crystallized ca. 189 Ma and cooled quickly to 500˚C in <5 Myrs. The adjacent McHugh Complex was deposited in the accretionary wedge of the arc, with input from both oceanic and accreted arc sources. McHugh Complex in this area consists of block-in-matrix mélange, with blocks of mudstone, chert, tuff, pillow lava, and rare limestone, that was metamorphosed to greenschist facies. It contains two distinct blocks of oceanic crust, one that is MORB and the other that formed in a within-plate setting. We interpret the latter to be the remnants of a seamount that was scraped off in the subduction channel and altered the dynamics of subduction in the area.

Dikes of the Sanak-Baranof near-trench magmatic belt intruded the McHugh Complex in this area during Eocene time (ca. 55 Ma), likely mobilizing hydrothermal fluids that reset $^{40}Ar/^{39}Ar$ ages of the seamount metavolcanics, obliterated pillow structures in the rim of the seamount metavolcanics tract, pervasively altered the mélange, and deposited sulfides throughout the mélange. These dikes cross-cut the regional shear fabric of the area, suggesting that both McHugh Complex and southward-adjacent Valdez Group rocks were in place in southern Alaska at the start of the Eocene epoch.

VII. Acknowledgements

The work presented here was supported by grants from the Geological Society of America, the Alaska Geological Society, and the University of Alaska Fairbanks. Meekin's Air Service flew us to the remote field area. Help in the field from Phoenix McDaniel, Veselina Yakimova, and Telayna Gordon (supported by an Undergraduate Research and Scholarly Activity—URSA—award from UAF) is gratefully acknowledged. We thank Karen Spaleta, Ken

Severin, and all the staff at UAF's Advanced Instrumentation Laboratory for help in acquiring and interpreting XRD and XRF data. Discussions with Jochen Mezger and John Wakabayashi helped guide our interpretations. We thank Mary Keskinen for comments that led to the improvement of the final manuscript. Finally, this project began with Gar and Jan Pessel, whose consistent help and dedication to geology have inspired and guided E. Nadin for the past several years.

VIII. References

Amato, J.M., and Pavlis, T.L. 2010. Detrital zircon ages from the Chugach terrane, southern Alaska, reveal multiple episodes of accretion and erosion in a subduction complex. Geology, **38**: 459–462. doi:10.1130/G30719.1.

Amato, J.M., Rioux, M.E., Kelemen, P.B., Gehrels, G.E., Clift, P.D., Pavlis, T.L., and Draut, A.E. 2007. U-Pb geochronology of volcanic rocks from the Jurassic Talkeetna Formation and detrital zircons from prearc and postarc sequences: Implications for the age of magmatism and inheritance in the Talkeetna arc. Geological Society of America Special Paper 431: 253–271. doi:10.1130/2007.2431(11).

Amato, J.M., Pavlis, T.L., Clift, P.D., Kochelek, E.J., Hecker, J.P., Worthman, C.M., and Day, E.M. 2013. Architecture of the Chugach accretionary complex as revealed by detrital zircon ages and lithologic variations: Evidence for Mesozoic subduction erosion in south-central Alaska. Bulletin of the Geological Society of America, **125**: 1891–1911. doi:10.1130/B30818.1.

Barker, F., Farmer, G.L., Ayuso, R.A., Plafker, G., and Lull, J.S. 1992. The 50 Ma granodiorite of the eastern Gulf of Alaska: Melting in an accretionary prism in the forearc. Journal of Geophysical Research. **97**: 6757-6778.

Bradley, D.C., and Miller, M.L. 2006. Field guide to south-central Alaska's accretionary complex, Anchorage to Seward. Alaska Geological Society Field Guide Series, Anchorage, Alaska.

Bradley, D.C., Haeussler, P.J., and Kusky, T.M. 1993. Timing of early Tertiary ridge subduction in southern Alaska. U.S. Geological Survey Bulletin 2068: 163-177.

Bradley, D.C., Kusky, T.M., Haeussler, P.J., Karl, S.M., and Donley, D.T. 1999. Geologic map of the Seldovia quadrangle, south-central Alaska, U.S. Geological Survey Open-File Report OFR 88-18B. 1 sheet, 1:250,000. Available from http://pubs.usgs.gov/of/1999/of99-018/.

Bradley, D.C., Parrish, R., Clendenen, W., Lux, D., Layer, P., Heizler, M., and Donley, D.T. 2000. New geochronological evidence for the timing of early Tertiary ridge subduction in southern Alaska. US Geological Survey Professional Paper 1615: 5–21.

Bradley, D.C., Haeussler, P., O'Sullivan, P., Friedman, R., Till, A., Bradley, J. D., and Trop, J. 2007. Detrital Zircon Geochronology of Cretaceous and Paleogene Strata Across the South-Central Alaskan Convergent Margin. U.S. Geological Survey Professional Paper 1760–F: 36. Available from http://pubs.usgs.gov/pp/1760/f/pp1760f.pdf.

Braun, J. 2005. Quantitative constaints on the rate of landform evolution derived from low-temperature thermochronology. Reviews in Mineralogy and Geochemistry, **58**: 351-374.

Burns, L.E. 1985. The Border Ranges ultramafic and mafic complex, south-central Alaska: cumulate fractionates of island-arc volcanics. Canadian Journal of Earth Science, **22**: 1020–1038.

Burns, L.E. 1996. Geology of part of the Nelchina River gabbronorite and associated rocks, south-central Alaska. U.S. Geological Survey Bulletin 2058: 32 p.

Burns, L.E., Pessel, G.H., Little, T.A., Pavlis, T.L., Newberry, R.J., Winkler, G.R., and Decker, J. 1991. Geology of the northern Chugach Mountains, southcentral Alaska. Alaska Division of Geological and Geophysical Surveys Professional Report 94.

Clark, S.H.B. 1973. The McHugh Complex of south-central Alaska. U.S. Geological Survey Bulletin 1372-D.

Clift P., and Vannucchi, P. 2004. Controls on tectonic accretion versus erosion in subduction zones: Implications for the origin and recycling of the continental crust. Reviews of Geophysics, **42**: 31 p. doi:10.1029/2003RG000127.

Cloos, M. 1993. Lithospheric buoyancy and collisional orogenesis: Subduction of oceanic plateaus, continental margins, island arcs, spreading ridges, and seamounts. Geological Society of America Bulletin, **105**: 715-737.

Cowan, D.S. 1978. Origin of blueschist-bearing chaotic rocks in the Franciscan Complex, San Simeon, California. Geological Society of America Bulletin, **89**: 1415–1423.

Cowan, D.S. 1985. Structural styles in Mesozoic and Cenozoic mélanges in the western Cordillera of North America. Geological Society of America Bulletin, **96**: 451–462. doi:10.1130/0016-7606(1985)96<451:SSIMAC>2.0.CO;2.

Dahl, P.S. 1997. A crystal-chemical basis for Pb retention and fission-track annealing systematics in U-bearing minerals, with implications for geochronology. Earth and Planetary Science Letters **150**: 277-90.

Davidson, C., and Garver, J.I. 2017. Age and origin of the Resurrection ophiolite and associated turbidites of the Chugach-Prince William terrane, Kenai Peninsula, Alaska. The Journal of Geology, **125**: 681-700. doi:10.1086/693926.

Dazé, A., Lee, J.K.W., and Villeneuve, M. 2003. An intercalibration study of the Fish Canyon sanidine and biotite $^{40}Ar/^{39}Ar$ standards and some comments on the age of the Fish Canyon Tuff. Chemical Geology, **199**: 111-127. doi:10.1016/S0009-2541(03)00079-2.

Dominguez, S., Malavieille, J., and Lallemand, S.E. 2000. Deformation of accretionary wedges in response to seamount subduction: Insights from sandbox experiments. Tectonics, **19**: 182-196.

Ehlers, T.A. 2005. Crustal thermal processes and the interpretation of thermochronometer data. Review of Mineralogy and Geochemistry, **58**: 315-350.

Gale, A., Dalton, C.A., Langmuir, C.H., Su, Y., and Schilling, J. 2013. The mean composition of ocean ridge basalts. Geochemistry Geophysics Geosystems, **14**: 489-518. doi:10.1029/2012GC004334.

Garver, J.I., and Davidson, C.M. 2015. Southwestern Laurentian zircons in Upper Cretaceous flysch of the Chugach-Prince William terrane in Alaska. American Journal of Science, **315**: 537-556. doi:10.2475/06.2015.02.

Hacker, B.R., Kelemen, P.B., Rioux, M., McWilliams, M.O., Gans, P.B., Reiners, P.W., Layer, P.W., Söderlund, U., and Vervoort, J.D. 2011. Thermochronology of the Talkeetna intraoceanic arc of Alaska: $^{40}Ar/^{39}Ar$, U-Th/He, Sm-Nd, and Lu-Hf dating. Tectonics, **30**: 1-23. doi:10.1029/2010TC002798.

Haeussler, P.J., Gehrels, G.E., and Karl, S.M. 2006. Constraints on the age and provenance of the Chugach accretionary complex from detrital zircons in the Sitka Graywacke near Sitka, Alaska. U.S. Geological Survey Professional Paper 1709-F.

Harrison, T.M. 1981. Diffusion of ^{40}Ar in hornblende. Contributions to Mineralogy and Petrology, **70**: 324-331.

Horton, J.W., Blake, D.E., Wylie, A.S., and Stoddard, E.F. 1986. Metamorphosed mélange terrane in the eastern Piedmont of North Carolina. Geology, **14**: 551–553.

Karl, S.M., Oswald, P.J., and Hults, C.P. 2015. Field guide to the Mesozoic arc and accretionary complex of South-Central Alaska, Indian to Hatcher Pass. Geological Society of America Cordilleran Section Guidebook, Anchorage, Alaska.

Knaack, C.M., Cornelius, S., and Hooper, P.R. 1994. Trace element analysis of rocks and minerals by ICP-MS. Washington State University, Geology Department, Open File Report.

Kochelek, E.J., Amato, J.M., Pavlis, T.L., and Clift, P.D. 2011. Flysch deposition and preservation of coherent bedding in an accretionary complex: Detrital zircon ages from the Upper Cretaceous Valdez Group, Chugach terrane, Alaska. Lithosphere, **3**: 265–274. doi:10.1130/L131.1.

Kuiper, K.F., Deino, A., Hilgen, F.J., Krijgsman, W., Renne, P.R., and Wijbrans, J.R. 2008. Synchronizing Rock Clocks of Earth History. Science, **320**: 500-504. doi:10.1126/science.1154339.

Kusky, T.M., Bradley, D.C., Haeussler, P.J., and Karl, S. 1997. Controls on accretion of flysch and mélange belts at convergent margins: Evidence from the Chugach Bay thrust and Iceworm mélange, Chugach accretionary wedge, Alaska. Tectonics, **16**: 855-878. doi:10.1029/97tc02780.

Lawson, A.C. 1895. Sketch of the geology of the San Francisco Peninsula, California. U.S. Geological Survey. Annual Report, **15**: 399-476.

Little, T.A. 1988. Tertiary tectonics of the Border Ranges fault system, north-central Chugach Mountains, Alaska: Sedimentation, deformation and uplift along the inboard edge of a subduction complex. Ph.D. dissertation, Department of Geology, Stanford University, Stanford, CA.

Little, T.A., and Naeser, C.W. 1989. Tertiary tectonics of the Border Ranges Fault System, Chugach Mountains, Alaska: Deformation and uplift in a forearc setting. Journal of Geophysical Research: Solid Earth, **94**: 4333–4359. doi:10.1029/JB094iB04p04333.

Lytwyn, J., Lockhart, S., Casey, J., and Kusky, T. 2000. Geochemistry of near-trench intrusives associated with ridge subduction, Seldovia Quadrangle, southern Alaska. Journal of Geophysical Research, **105**: 27957-27978.

Mackevett, E., and Plafker, G. 1974. The Border Ranges fault of south-central Alaska. Journal of Research of the U.S. Geological Survey, **2**: 323-329.

McCulloch, M.T., and Gamble, J.A. 1991. Geochemical and geodynamical constraints on subduction zone magmatism. Earth and Planetary Science Letters, **102:** 358–374.

McDougall, I., and Harrison, T.M. 1988. Geochronology and thermochronology by the $^{40}Ar/^{39}Ar$ method. Oxford University Press, N.Y.

Meschede, M. 1986. A method of discriminating between different types of mid-ocean ridge basalts and continental tholeiites with the Nb-Zr-Y diagram. Chemical Geology, **56**: 207–218. doi:10.1016/0009-2541(86)90004-5.

Morris, J.D., and Hart, S.R. 1983. Isotopic and incompatible trace element constraints on the genesis of island arc volcanics from Cold Bay and Amak Island, Aleutians, and implications for mantle structure. Geochimica et Cosmochimica Acta, **47**: 2051–2030.

Mulcahy, S.R., Starnes, J.K., Day, H.W., Coble, M.A., and Vervoort, J.D. 2018. Early onset of Franciscan subduction. Tectonics, **37**: 1194-1209. doi:10.1029/2017TC004753.

Nelson, S.W., and Blome, C.D. 1991. Preliminary geochemistry of volcanic rocks from the McHugh Complex and Kachemak terrane, southern Alaska. U.S. Geological Survey Open-File Report 91-134: 1–14.

Nelson, S.E., Blome, C.D., and Karl, S.M. 1987. Late Triassic and Early Cretaceous fossil ages from the McHugh Complex, southern Alaska. U.S. Geological Survey Circular 998: 96-98.

Pavlis, T.L. 1982. Origin and age of the Border Ranges Fault of southern Alaska and its bearing on the Late Mesozoic tectonic evolution of Alaska. Tectonics, **1**: 343–368. doi:10.1029/TC001i004p00343.

Pavlis, T.L., and Roeske, S.M. 2007. The Border Ranges fault system, southern Alaska. Geological Society of America Special Paper 431: 95–127. doi:10.1130/2007.2431(05).

Pearce, J.A., and Cann, J.R. 1973. Tectonic setting of basic volcanic rocks determined using trace element analyses. Earth and Planetary Science Letters, **19**: 290–300. doi:10.1016/0012-821X(73)90129-5.

Pearce, J.A., and Norry, M.J. 1979. Petrogenetic implications of Ti, Zr, Y, and Nb variations in volcanic rocks. Contributions to Mineralogy and Petrology, **69**: 33–47. doi:10.1007/BF00375192.

Pessel, G.H., Henning, M.W., and Burns, L.E. 1981. Preliminary geologic map of parts of the Anchorage C-1, C-2, D-1, and D-2 quadrangles, Alaska. Alaska Division of Geological and Geophysical Surveys, Open-file Report AOF-121. 1 sheet, scale 1:63,360.

Plafker, G., and Berg, H.C. 1994. Overview of the geology and tectonic evolution of Alaska. The Geology of Alaska: Geological Society of America. pp. 989–1021. Available from http://www.dggs.alaska.gov/pubs/id/22261.

Plafker, G., Nokleberg, W.J., and Lull, J.S. 1989. Bedrock geology and tectonic evolution of the Wrangellia, Peninsular, and Chugach terranes along the Trans-Alaska Crustal Transect in the Chugach Mountains and southern Copper River basin, Alaska. Journal of Geophysical Research, **94**: 4255–4295.

Plafker, G., Moore, J.C., and Winkler, G.R. 1994. Geology of the southern Alaska margin. The Geology of Alaska: Geological Society of America. pp. 389–449. Available from http://www.dggs.alaska.gov/pubs/id/22261.

Rioux, M., Hacker, B., Mattinson, J., Kelemen, P., Blusztajn, J., and Gehrels, G. 2007. Magmatic development of an intra-oceanic arc: High-precision U-Pb zircon and whole-rock isotopic analyses from the accreted Talkeetna arc, south-central Alaska. Geological Society of America Bulletin, **119**: 1168–1184. doi:10.1130/B25964.1.

Roeske, S.M., Mattinson, J.M., Armstrong, R.L. 1989. Isotopic ages of glaucophane schists on the Kodiak Islands, southern Alaska, and their implications for the Mesozoic tectonic history of the Border Ranges fault system. Geological Society of America Bulletin, **101**: 1021-1037.

Saunders, A.D., Norry, M.J., and Tarney, J. 1991. Fluid influence on the trace element composition of subduction zone magmas. Philosophical Transactions of the Royal Society, **335**: 377–392. doi:10.1098/rsta.1991.0053.

Sun, S., and McDonough, W.F. 1989. Chemical and isotopic systematics of oceanic basalts: implications for mantle composition and processes. Geological Society, London, Special Publications, **42**: 313–345. doi:10.1144/GSL.SP.1989.042.01.19.

Tafti, R., Mortensen, J.K., Lang, J.R., Rebagliati, M. and Oliver, J.L. 2009. Jurassic U-Pb and Re-Os ages for newly discovered Xietongmen Cu-Au porphyry district, Tibet: Implications for metallogenic epochs in the southern Gangdese Belt. Economic Geology, **104**: 127-136. doi:10.2113/gsecongeo.104.1.127/

Trop, J.M., and Ridgway, K.D. 2007. Mesozoic and Cenozoic tectonic growth of southern Alaska: A sedimentary basin perspective. Geological Society of America Special Paper 431: 55-94. doi:1130/2007.2431(04).

Wakabayashi, J. 2015. Anatomy of a subduction complex: architecture of the Franciscan Complex, California, at multiple length and time scales. International Geology Review, **57**: 669-746. doi:10.1080/00206814.2014.998728.

Wilson, F.H., Hults, C.P., Mull, C.G., and Karl, S.M., comps. 2015. Geologic map of Alaska. U.S. Geological Survey Scientific Investigations Map 3340, 197 p., 2 sheets, scale 1:584,000. doi:10.3133/sim3340.

Winchester, J.A., and Floyd, P.A. 1977. Geochemical discrimination of different magma series and their differentiation products using immobile elements. Chemical Geology, **20**: 325–343.

Wood, D.A. 1980. The application of a Th-Hf-Ta diagram to problems of tectonomagmatic classification and to establishing the nature of crustal contamination of basaltic lavas of the British Tertiary Volcanic Province. Earth and Planetary Science Letters, **50**: 11–30. doi:10.1016/0012-821X(80)90116-8.

Yakimova, V., and Nadin, E.S. 2017. Field study of the Border Ranges fault system in southwestern Alaska. Poster presentation, EarthScope National Meeting, May 16-18, Anchorage, AK.

Table 1: Summary of compositional data for igneous rocks in the Nelchina mélange and in the adjacent Talkeetna volcanic arc mid-crustal section.

	150715-12 (pillow basalt)	16Ba03 (trachy-andesite)	16Ba06 (trachy-basalt)	16Ba07 (trachy-basalt)	16Ba10 (trachy-basalt)	16Ba16 (trachy-basalt)	16Ba24 (trachy-basalt)	16Ba02 (felsite)	16Ba21 (amphi-bolite)
SiO_2	42	62	46	44	48	45	40	66	49
TiO_2	3.7	0.8	2.8	3.0	3.2	2.1	3.3	0.3	1.5
Al_2O_3	12	15	15	15	16	13	14	16	11
Fe_2O_3[a]	13	7	11	13	11	15	14	2	18
MnO	0.1	0.1	0.1	0.2	0.1	0.4	0.2	0.0	0.2
MgO	11	1.9	5.9	5.8	5.6	7.2	6.1	3.1	10
CaO	5.9	2.2	10	8.1	6.5	8.6	10	1.2	7.7
Na_2O	3.5	5.8	2.8	2.4	2.8	2.1	1.6	4.8	1.1
K_2O	1.1	3.1	1.6	2.5	3.0	0.2	2.1	0.9	0.2
P_2O_5	0.7	0.2	0.4	0.6	0.5	0.2	0.8	0.1	0.2
Sum	92.5	98.1	96.1	95.2	96.5	93.0	92.1	94.5	97.9
LOI	6.2	1.9	5.6	4.3	4.5	10.0	5.9	5.9	1.7
Total	98.7	100.0	101.7	99.4	100.9	103.0	97.9	100.4	99.6
Rb	8.4	21	14	25	30	6.2	25	20	0.9
Sr	520	270	560	570	590	270	690	310	210
Ba	390	1700	840	1000	870	140	820	230	44
Cs	0.7	1.4	1.0	0.6	1.6	0.8	1.3	2.8	0.3
Pb	2.3	6.3	2.3	2.4	2.4	2.3	2.4	3.2	1.8
Y	31	41	26	29	27	43	32	6	41
Zr	270	500	270	270	310	120	300	110	90
Hf	6.6	13	6.1	6.9	7.7	3.3	7.6	2.9	2.4
Nb	26	40	38	24	25	4.0	26	1.2	4.7
Ta	1.7	2.4	2.4	1.5	1.6	0.3	1.7	0.1	0.3
Th	1.6	2.5	3.0	1.4	1.4	0.3	1.5	0.8	0.4
U	0.9	0.9	1.0	0.6	0.5	0.1	0.7	0.5	0.2
La	25	47	31	28	28	4.8	27	4.9	7.2
Ce	61	103	66	64	67	13	64	12	18
Pr	9.0	14	8.6	9.1	9.5	2.3	9.3	1.7	2.6
Nd	40	57	36	40	41	12	42	7.0	12
Sm	9.4	11.7	8.2	9.1	9.0	4.5	9.9	1.7	3.9
Eu	3.1	4.9	2.7	3.5	3.0	1.23	3.4	0.52	1.3
Gd	8.5	9.8	7.3	8.2	7.7	6.0	8.5	1.5	5.1
Tb	1.26	1.5	1.08	1.21	1.13	1.16	1.28	0.21	0.99
Dy	6.8	8.7	5.9	6.5	6.2	7.8	7.2	1.2	7.0
Ho	1.24	1.6	1.08	1.20	1.11	1.68	1.28	0.23	1.6
Er	3.0	4.1	2.7	2.9	2.7	4.8	3.2	0.60	4.6
Tm	0.40	0.57	0.35	0.38	0.36	0.71	0.42	0.09	0.70
Yb	2.3	3.5	2.0	2.2	2.1	4.3	2.4	0.54	4.7
Lu	0.34	0.52	0.31	0.33	0.30	0.71	0.35	0.08	0.75
Ni[b]	36	3	140	60	60	60	60	10	60
V[b]	280	30	140	200	180	1200	550	20	270
Cr[b]	120	13	120	120	120	130	150	4	70
Sc	25	11	16	23	21	44	24	3.9	51

NOTE: Major and minor elements measured using X-ray fluorescence (XRF) at University of Alaska Fairbanks (UAF) Advanced Instrumentation Laboratory (AIL). Oxides and LOI are in wt%. Trace and REEs are in ppm. Analytical errors are 10% RSD except REEs, which are 5% RSD.

a) Fe_2O_3 is total Fe recalculated as Fe^{3+}.

b) All trace elements measured using ICP-MS at Washington State University Peter Hooper GeoAnalytical Laboratory except these, which were measured using XRF at UAF AIL.

Figures

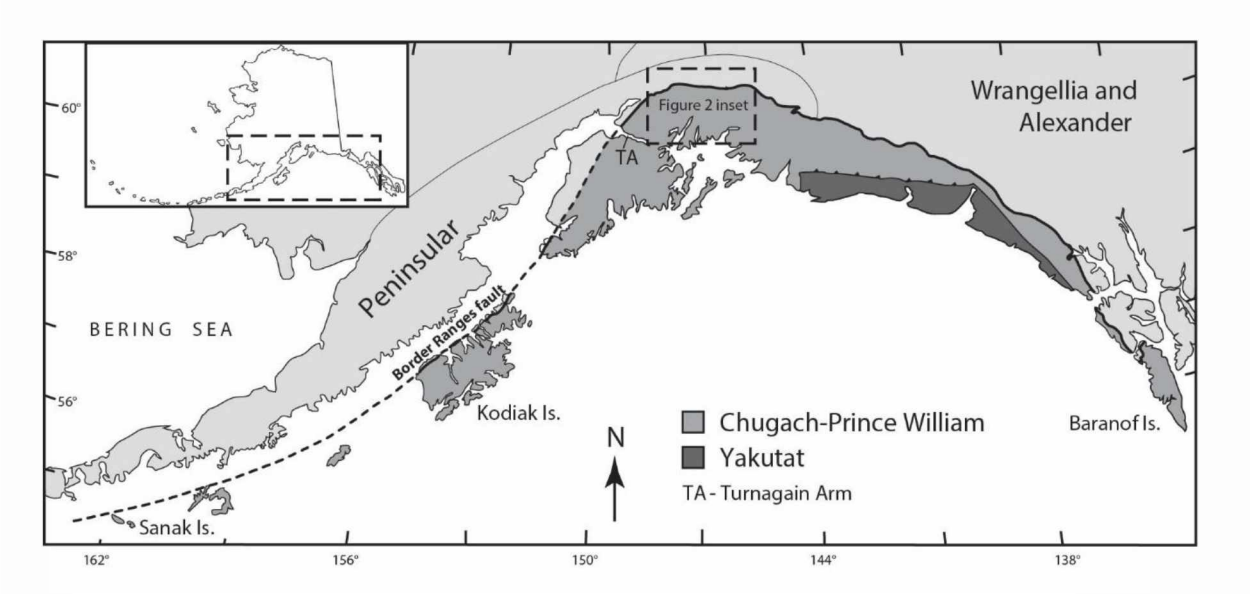

Figure 1: Map showing the general terrane configuration of southern Alaska. The Border Ranges fault (BRF) is thought to be the subduction megathrust boundary between the Talkeetna arc (Peninsular terrane) and the McHugh mélange–Valdez Group flysch (Chugach terrane/accretionary complex). The dashed box shows the location of the inset in Figure 2. (Modified from Garver and Davison 2015.)

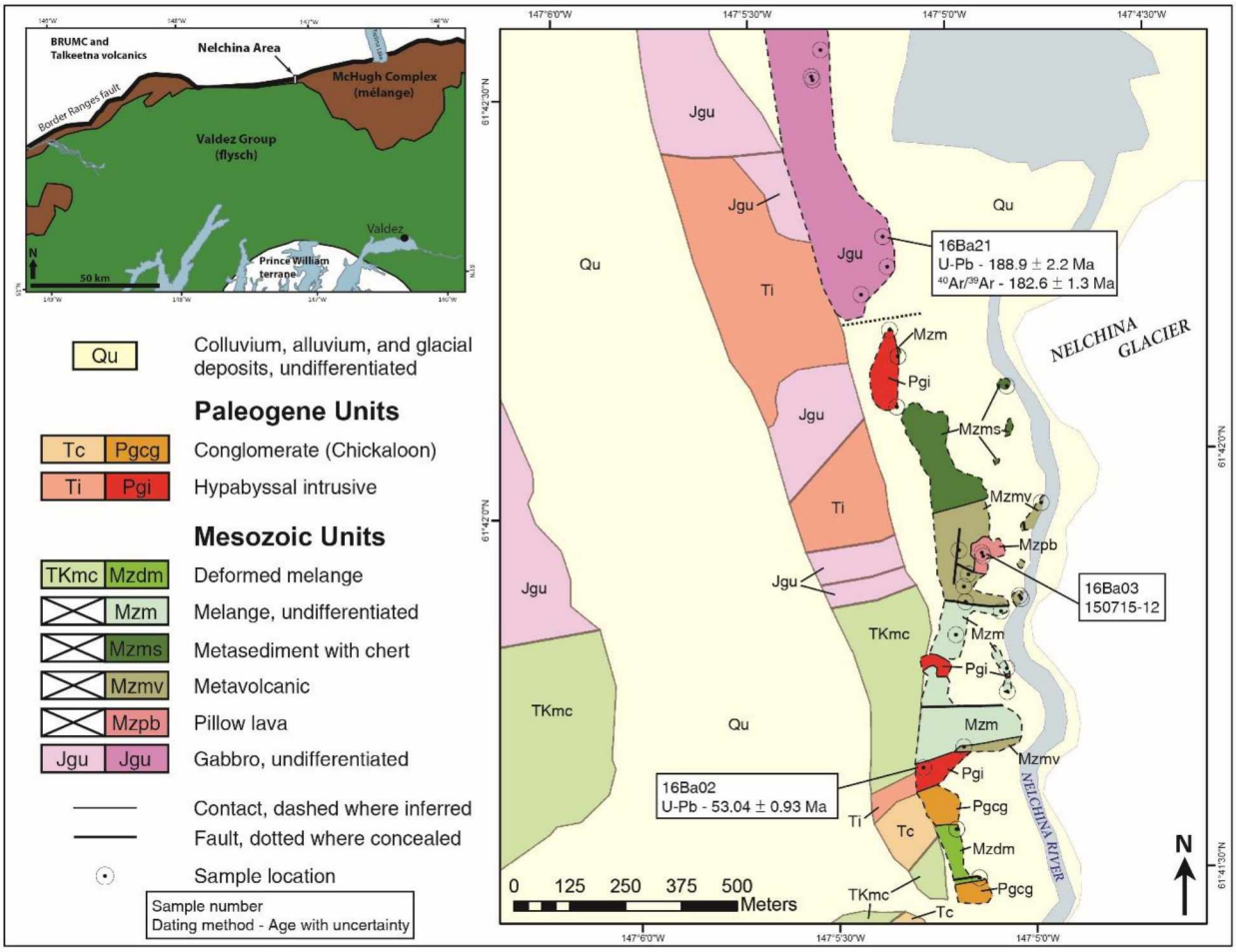

Figure 2: Map of Nelchina area mélange showing recently exposed bedrock mapped in this study (see text for unit descriptions). Names, descriptions, and unit ages are generally adopted from Burns et al. (1991), whose mapping is copied here along the western edge of the map area in paler shades and with solid contacts. A blank legend item means there was no correlative unit. All sample locations discussed in the text are marked. New ages and their types are indicated by boxes. Samples 150715-12 and 16Ba03 yielded inconclusive $^{40}Ar/^{39}Ar$ ages, but their locations are marked on the map.

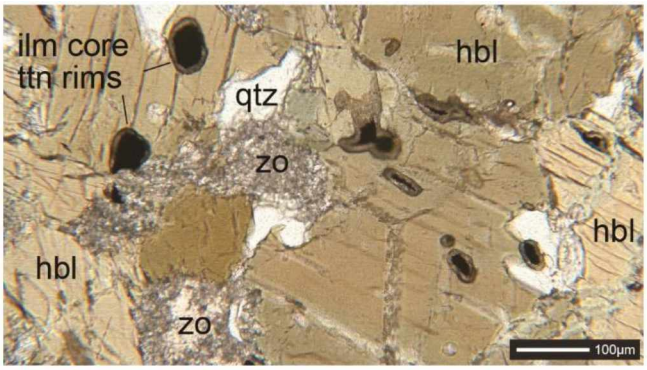

Figure 3: Photomicrograph of amphibolite sample 16Ba21 from the Talkeetna arc exposure at the southernmost part of the Peninsular terrane in the study area. Hornblende (hbl) constitutes ~80% of the sample. The remainder is sausseritized plagioclase (zo – zoisite), quartz (qtz), and ilmenite (ilm) with titanite (ttn) reaction rims.

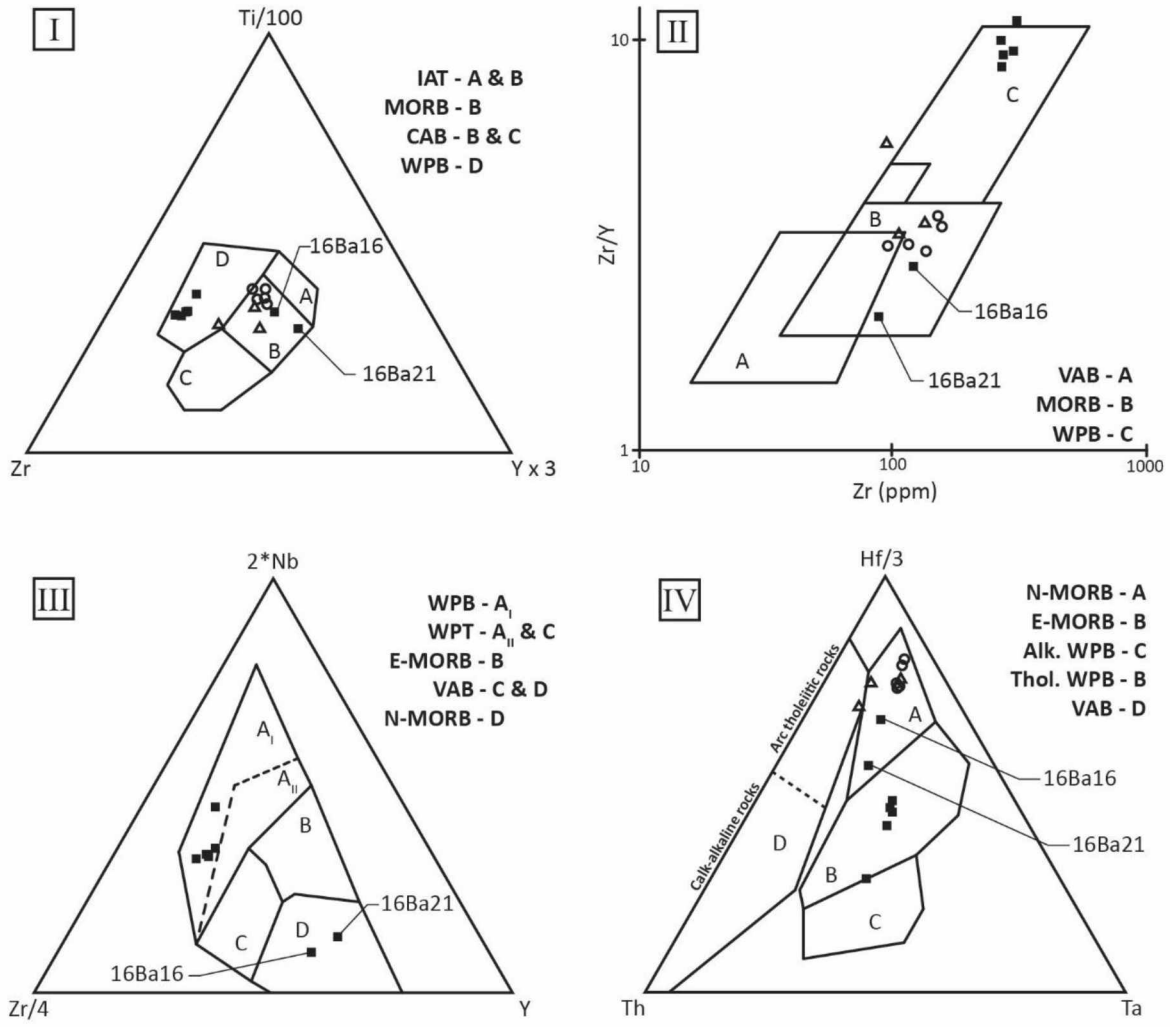

Figure 4: Tectonic discrimination diagrams for sampled basalts showing that the trachybasalts from within the mélange have primarily within-plate origins, except for sample 16Ba16 which plots as N-MORB. Sample 16Ba21 also plots as N-MORB, but it is an amphibolite from the Talkeetna arc, rather than a trachybasalt block in the mélange. In I, II, and IV, filled squares are data from this study, open circles are data from Plafker et al. (1989), and open triangles are from Nelson and Blome (1991). Only samples from this study plotted in III, as Nb in samples from the literature were below detection values. I) Ti-Zr-Y diagram after Pearce and Cann (1973). II) Zr/Y-Y diagram after Pearce and Norry (1979). III) Zr-Y-Nb diagram after Meschede (1986).

IV) Th-Hf-Ta diagram after Wood (1980). IAT – island arc tholeiite, MORB – mid-ocean ridge basalt, CAB – calk-alkaline basalt, WPB – within-plate basalt, VAB – volcanic arc basalt, WPT – within-plate tholeiite, E-MORB – enriched MORB, N-MORB – normal MORB.

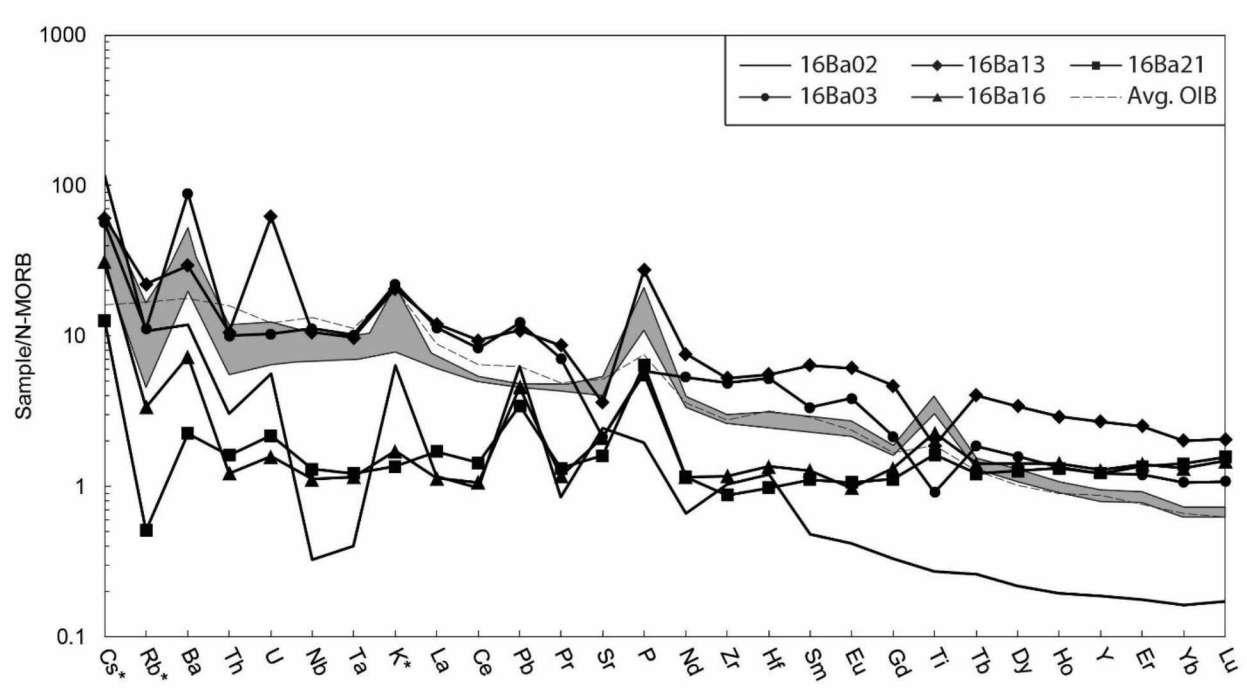

Figure 5: Spider diagram of trace and rare-earth element data sorted by increasing compatibility, after Sun and McDonough (1989). Starred elements are especially mobile. The shaded area spans all within-plate trachybasalts in the area that are genetically related. Diagram normalized to normal-MORB (N-MORB) concentrations from Gale et al. (2013). Also plotted is an average ocean island basalt (OIB—dashed line) composition from Sun and McDonough (1989) in order to compare within-plate basalt volcanic rocks from Nelchina to the average.

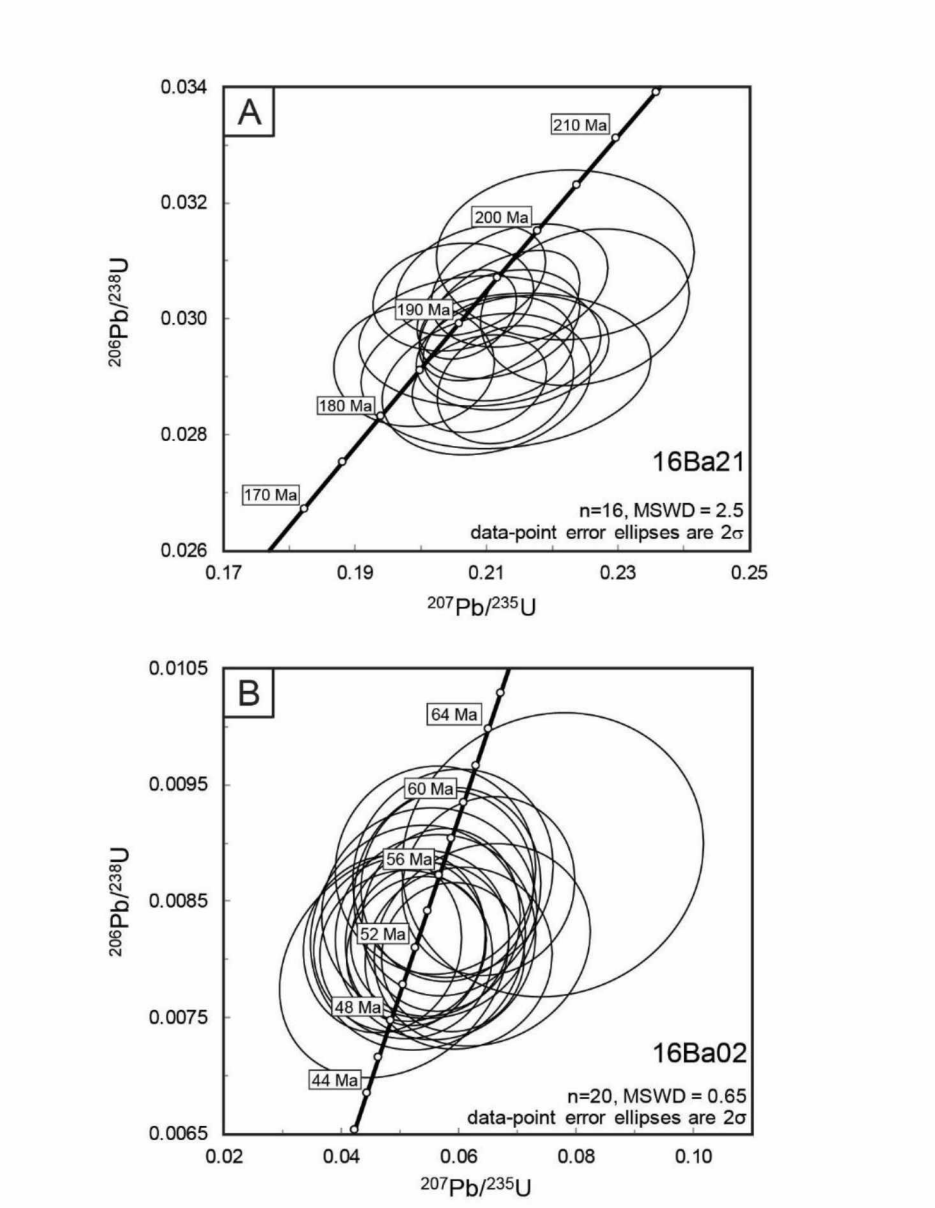

Figure 6: Concordia plots of zircon U-Pb analyses for samples 16Ba21 and 16Ba02, with ellipses showing 2σ error. A) 16 zircons from amphibolite sample 16Ba21 from the southernmost Talkeetna arc exposure in the area cluster on a concordia of 189.9 ± 2.2 Ma. B) 20 zircons from sample 16Ba02 from a hypabyssal dike crosscutting the mélange cluster on a concordia of 53.04 ± 0.93 Ma.

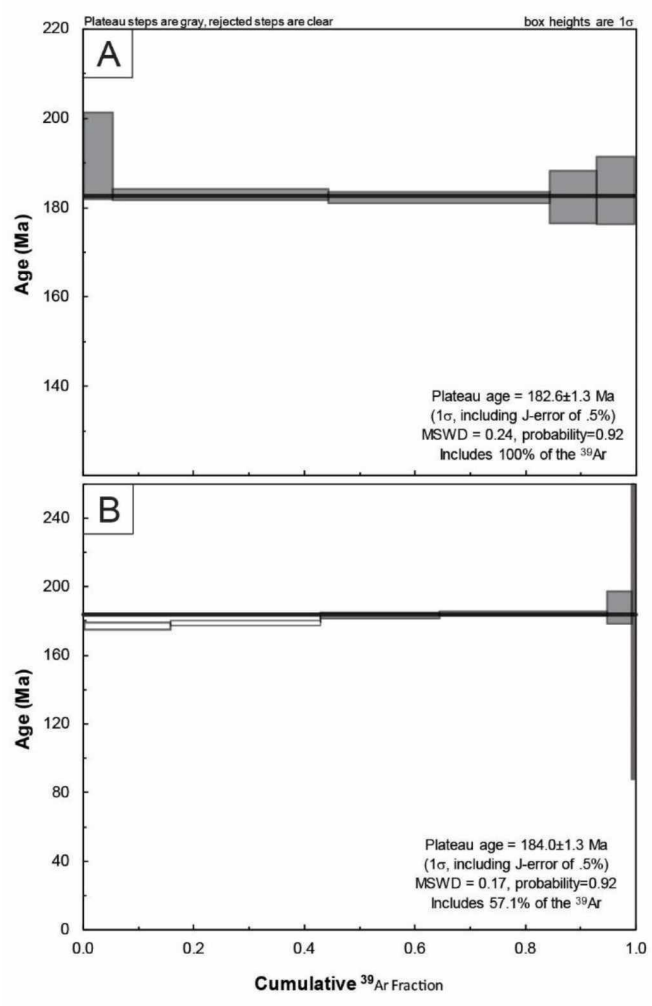

Figure 7: $^{40}Ar/^{39}Ar$ plateau ages for two rocks from the southernmost BRUMC. A) Sample 16Ba21 (amphibolite from the base of the Talkeetna arc) hornblende $^{40}Ar/^{39}Ar$ plateau age is 182.6 ± 1.3 Ma. B) Sample 16Ba28 (gabbro from the base of the Talkeetna arc) hornblende $^{40}Ar/^{39}Ar$ plateau age is 184.0 ± 1.3 Ma.

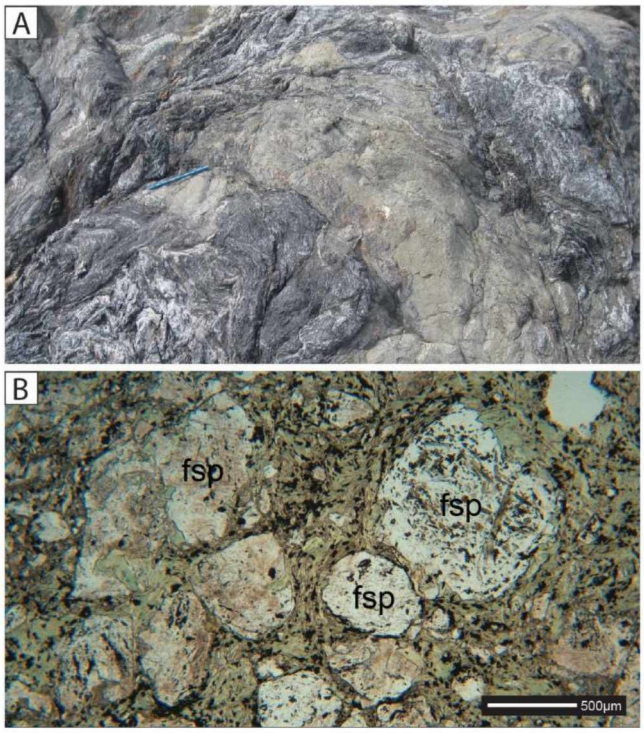

Figure 8: Photos showing the relationships between mélange mudstone and chert (Mzms) at different scales. A) Folded white-gray ribbon chert that includes layers of green tuff. B) Tuffaceous material in thin section (plane polarized light) shows chlorite grew around large alkali feldspar clasts.

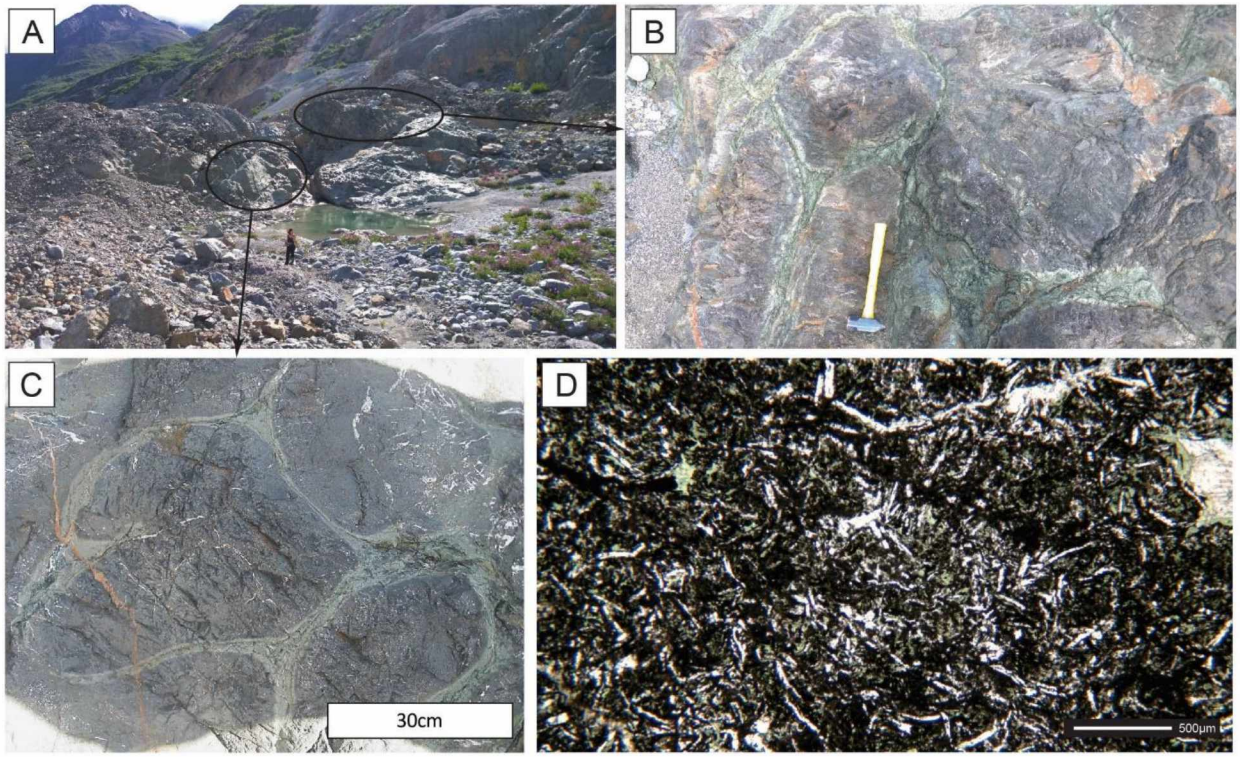

Figure 9: Outcrop and thin section pictures of the pillow-lava block within the Nelchina mélange. A) Overview of the block, indicating the locations of the photos shown in (B) and (C). Block is ~200m by 250m. B) The upper part of the outcrop, where sample 16Ba03 was taken, is a pillow trachyandesite. The pillow structures are less well preserved than lower in the outcrop. (Hammer for scale is 35cm long.) C) The lower part of the outcrop, from which sample 150715-12 was taken, is well-preserved but altered pillow basalt. Each pillow is ~1m in diameter. D) Photomicrograph taken in plane-polarized light of sample 150715-12 showing randomly oriented plagioclase laths. These laths have been preserved as secondary albite and have not been aligned by shearing.

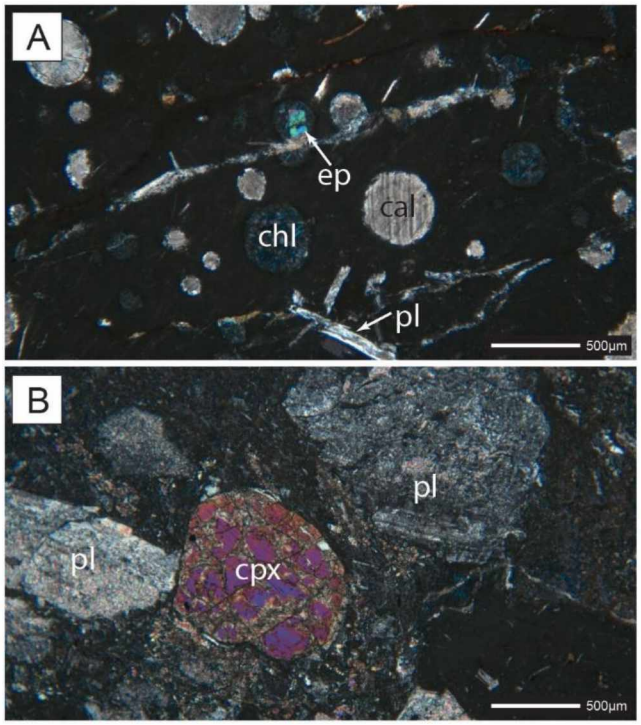

Figure 10: Photomicrographs of trachybasalt sample 16Ba07, taken in cross-polarized light, showing greenschist facies index minerals (chlorite and epidote) and degree of alteration. A) Vesicles are filled with calcite, chlorite, epidote, and quartz. Plagioclase laths are preserved in the groundmass between the vesicles. B) Larger grains of clinopyroxene and plagioclase still preserved. Plagioclase has altered almost completely to sericite.

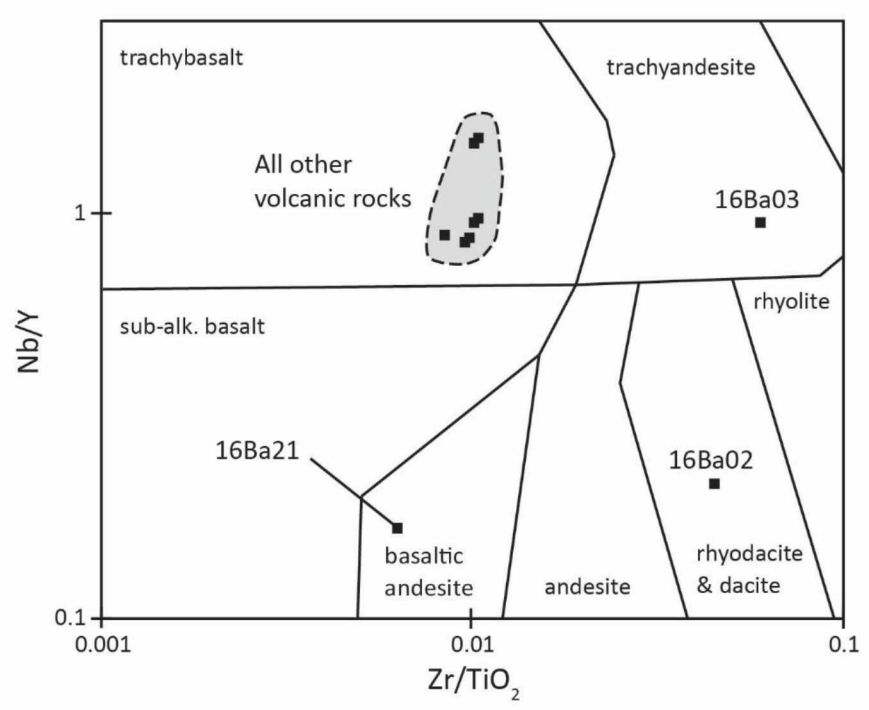

Figure 11: Classification diagram for igneous rocks based on immobile elements after Winchester and Floyd (1977). Sample 16Ba03 (upper pillow lava) plots as a trachyandesite is significantly more felsic than other volcanic rocks in the study area, which are trachybasalts. Sample 16Ba02 (cross-cutting felsite dike) plots as a dacite. Sample 16Ba21 (amphibolite) plots as a basaltic andesite. Diagram has been rotated 90 degrees and mirrored from the original diagram to more easily be an analog to total alkali vs silica diagram.

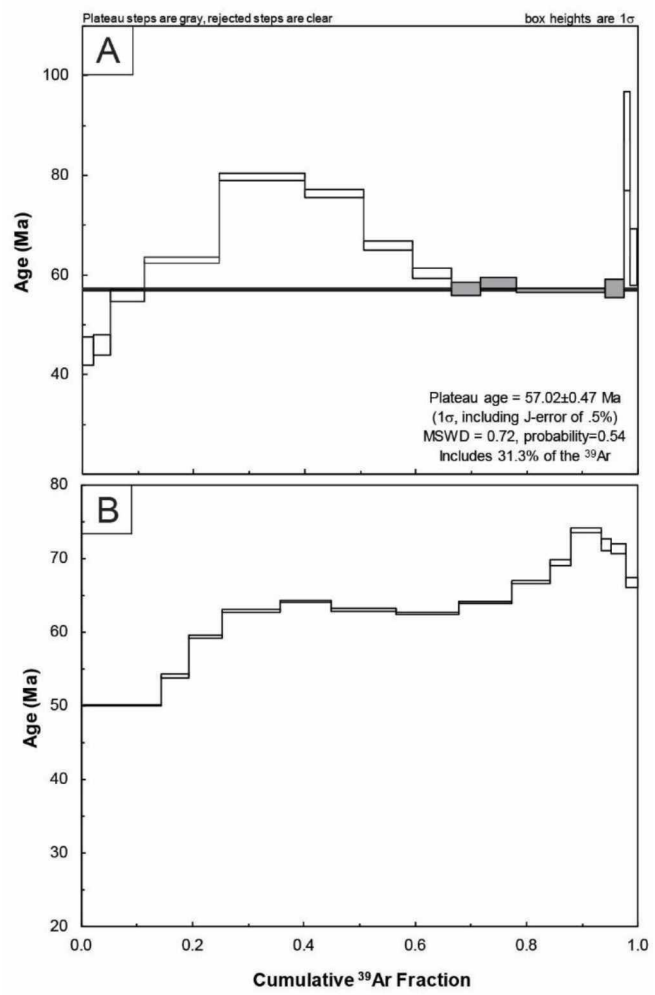

Figure 12: Whole-rock $^{40}Ar/^{39}Ar$ plateaus from pillow-lava samples A) 150715-12 (basalt) and B) 16Ba03 (trachyandesite). Sample 150715-12 yielded a saddle age of 57.02 ± 0.47 Ma based on 31.3% of the ^{39}Ar. Sample 16Ba03 yielded a saddle age of 61.7 ± 1.7 Ma at ~35% of Ar released. See text for interpretations of these results.

Figure 13: Outcrop photo of the sample location of 16Ba02, which shows the southernmost cross-cutting felsite dike (Pgi). This dike, along with two others in the field area, are related to Sanak-Baranof plutonism. Black bear for scale. McHugh Complex mesomélange visible on right side of photo.

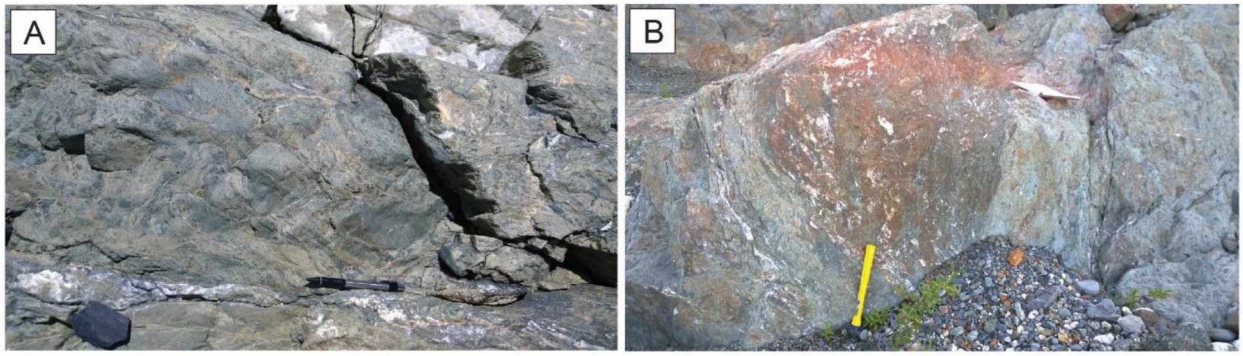

Figure 14: Outcrop photos that show examples of the mudstone matrix of the McHugh Complex in the Nelchina area. A) The block-in-matrix structure typical of mélange is displayed here at a larger scale, showing the scale independence of mélange. Pencil is 10cm in length. B) The mélange block-in-matrix structure displayed at a smaller scale. Hammer is 35cm in length.

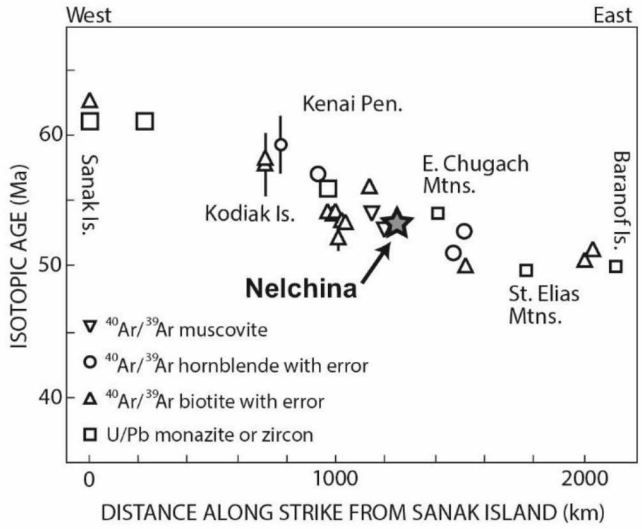

Figure 15: Trend of pluton ages throughout the Sanak-Baranof belt. Star indicates the location of dated felsite dike that cross-cuts the Nelchina mélange, which fits in well with the established trend. Distance on x-axis is distance along strike of the Border Ranges fault (BRF). Modified from Bradley et al. (2000).

Appendix ($^{40}Ar/^{39}Ar$ methodology)

Standards and unknowns were placed in 2mm deep wells in 18mm diameter aluminum disks, with standards placed strategically so that the lateral neutron flux gradients across the disk could be evaluated. Planar regressions were fit to the standard data, and the $^{40}Ar/^{39}Ar$ neutron fluence parameter, J, interpolated for the unknowns. Uncertainties in J are estimated at 0.1 - 0.2% (1σ), based on Monte Carlo error analysis of the planar regressions (Best et al. 1995). All specimens were irradiated in the Cadmium-lined, in-core CLICIT facility of the Oregon State University TRIGA reactor. The duration of irradiation was 10 hours and using the Fish Canyon sanidine (28.2 Ma; Kuiper et al. 2008) and GA1550 biotite (98.5 Ma; Spell and McDougall 2003) standards.

Irradiated samples were placed in a Cu sample tray, with a KBr cover slip, in a stainless steel high-vacuum extraction line and baked with an infrared lamp for 24 hours. Single crystals and pieces of whole rock were either fused or step heated using the laser, and reactive gases were removed, after ~3 minutes, by three NP-10 SAES getters (two at room temperature and one at 450°C) prior to being admitted to an ARGUSVI mass spectrometer by expansion. Five argon isotopes were measured simultaneously over a period of 6 minutes. Measured isotope abundances were corrected for extraction-line blanks, which were determined before every sample analysis. Line blanks averaged ~4.500 fA for mass 40 and ~0.016 fA for mass 36.

Mass discrimination was monitored by online analysis of air pipettes and gave a mean of $D = 1.01085 \pm 0.00043$ per amu, based on 52 aliquots interspersed with the unknowns. A value of 295.5 was used for the atmospheric $^{40}Ar/^{36}Ar$ ratio (Steiger and Jäger 1977) for the purposes of routine measurement of mass spectrometer discrimination using air aliquots, and correction for atmospheric argon in the $^{40}Ar/^{39}Ar$ age calculation. Corrections are made for neutron-induced

^{40}Ar from potassium, ^{39}Ar and ^{36}Ar from calcium, and ^{36}Ar from chlorine (Roddick 1983; Renne et al. 1998; Renne and Norman 2001). Data collection was performed using Pychron (Ross 2017), and data reduction, error propagation, age calculation, and plotting were performed using MassSpec software (version 8.091; Deino 2013). The decay constants used were those recommended by Steiger and Jäger (1977).

References for Appendix

Best, M.G., Christiansen, E.H., Deino, A.L., Grommé, C.S., and Tingey, D.G. 1995. Correlation and emplacement of a large, zoned, discontinuously exposed ash flow sheet; the $^{40}Ar/^{39}Ar$ chronology, paleomagnetism, and petrology of the Pahranagat Formation, Nevada. J. Geophys. Res. 100, 24593-24609.

Dazé, A., Lee, J.K.W., and Villeneuve, M. 2003. An intercalibration study of the Fish Canyon sanidine and biotite $^{40}Ar/^{39}Ar$ standards and some comments on the age of the Fish Canyon Tuff. Chem. Geol. 199, 111-127.

Deino, A.L. 2013. Users manual for Mass Spec v. 7.961: Berkeley Geochronology Center Special Publication 1a, 132 p.

Kuiper, K.F., Deino, A., Hilgen, F.J., Krijgsman, W., Renne, R., and Wijbrans, J.R. 2008. Synchronizing Rock Clocks of Earth History. Science 320, 500-504.

Renne, P.R., Cassata, W.S., and Morgan, L.E. 2009. The isotopic composition of atmospheric argon and $^{40}Ar/^{39}Ar$ geochronology: Time for a change? Quatern. Geochronol. 4, 288-298.

Renne, P.R., and Norman, E.B. 2001. Determination of the half-life of 40Ar by mass spectrometry. Phys. Rev. C 63 (047302), 3.

Renne P.R., Swisher C.C., Deino A.L., Karner D.B., Owens T.L. and DePaolo D.J. 1998. Intercalibration of standards, absolute ages and uncertainties in $^{40}Ar/^{39}Ar$ dating. Chem. Geol. 145, 117-152.

Ross, J. 2017. https://github.com/NMGRL/pychron. DOI 10.5281/zenodo.9884.

Roddick, J.C. 1983. High precision intercalibration of ^{40}Ar-^{39}Ar standards. Geochim. Cosmochim. Acta 47, 887-898.

Steiger R.H. and Jäger E. 1977. Subcommission on geochronology: convention on the use of decay constants in geo- and cosmochronology. Earth Planet. Sci. Lett. 36, 359-362.

Spell T.L. and McDougall I. 2003. Characterization and calibration of $^{40}Ar/^{39}Ar$ dating standards. Chem. Geol. 198, 189-211.

Chapter 3: Conclusion

Three primary goals motivated this project:

1. Map and sample newly revealed mélange exposures at the base of Nelchina Glacier in order to provide a framework for analyses,
2. Characterize these exposures in order to describe variability in the McHugh Complex,
3. Determine timing constraints for accretion and subsequent disruption of the McHugh Complex in this area.

The new map is presented in Figure 2 of Chapter 2, which is a submitted manuscript. The map shows that mesomélange is more prevalent towards the southern end of the exposure, where it is in contact with the Valdez Complex. I interpreted some of this deformation to be due to progressive stratal disruption inherent to Type II tectonic mélange (from Cowan 1985). In addition, I mapped and analyzed pillow lavas that I interpreted (Chapter 2) to be the decapitated remains of a seamount, which probably played a role in the disruption of the mélange as they were being subducted.

Rock characterization (point 2) resulted from substantial geochemical analyses for nine samples and petrographic analyses at the outcrop, hand sample, and thin section scales. The large block of volcanic rocks in the middle of the Nelchina mélange (Figures 2 and 9) has a within-plate signature (Figure 4), which led to the interpretation that this block was part of a seamount that became incorporated into the mélange. Other blocks within the mélange are part of typical ocean plate stratigraphy—N-MORB (Figures 4 and 5), chert, and mudstone, all metamorphosed to greenschist facies. Based on these facts, I interpret the McHugh Complex as a tectonic mélange, which shows progressively deformed ocean plate stratigraphy metamorphosed under the same temperature and pressure conditions (Wakabayashi 2015).

The McHugh Complex has variable outcrop thickness, and is not present at all in some parts of the Chugach terrane (Figure 2 inset). This variation is caused by both strike-slip faulting along the BRF and topographic effects. The mélange in the Nelchina area is a particularly thin exposure of McHugh Complex. The exposures in this area, however, are different in many ways from the McHugh as typically described by others. Here, the metamorphic grade is greenschist facies instead of prehnite-pumpellyite as reported elsewhere (e.g. Clark 1973, Burns et al. 1991, Bradley et al. 1993). Clark (1973) noted the presence of sandstones in both the type and reference localities of the McHugh Complex, but sandstones are entirely absent in the Nelchina mélange. Finally, pillow lavas are rare in the McHugh Complex, and pillow trachyandesites have never been reported in the complex. The differences in metamorphic grade could mean this area of mélange was subducted more deeply than other parts of the McHugh Complex before being uplifted and exhumed; it could also mean that this part of the McHugh Complex has been overprinted by a later metamorphic event. I favor the former, as there is no uniform pervasive foliation. The presence of basalt, chert, and mudstone, and the lack of sandstone in the Nelchina area could mean that the sandstone was tectonically eroded away during one or more events suggested by Amato and Pavlis (2010) or Amato et al. (2013). It could also mean that this particular part of the mélange was not close enough to sedimentary input for there to be sand-sized clasts.

Finally, I was able to assign ages to geological events in the area (point 3) by applying zircon U-Pb dating on three samples, and hornblende and whole-rock $^{40}Ar/^{39}Ar$ dating on four samples. The upper limit of accretion and deformation is set by two new ages on an amphibolite that is exposed to the north just across the BRF from the McHugh Complex. These ages indicate that the zircon crystallization age of this part of the arc is ~189 Ma, and it cooled through

amphibole closure temperature of 550°C by ~182 Ma. The latter age could represent the natural cooling age of the rock, or it could record the timing of exhumation of this part of the arc. The age of the Nelchina cross-cutting dikes fits in well with the established trend of near-trench pluton ages across southern Alaska (Figure 15), which are associated with spreading ridge subduction (e.g. Bradley et al. 1993, Lytwyn et al. 2000, Garver and Davidson 2015). Since these intrusions are undeformed and cross-cut both the mélange and the arc basement, it is likely that the Peninsular and Chugach terranes had to be in their current configuration before Sanak-Baranof related plutons were intruded into these rocks in the Eocene. While ages on the seamount were inconclusive, they likely point to a partial resetting event that is coeval with the intrusion of three Sanak-Baranof plutons into the mélange.

Future Work

Due to the complex nature of the exposures in this area (and in all mélanges), there is room for more study to more fully understand this part of the accretionary complex. A larger scale map would more fully show the relationships between blocks within the mélange and in more detail. A detailed mapping project, especially in the mesomélange unit, should be at 1:5000 scale or larger. This map could confirm disruption of the mélange that may be due to seamount subduction or shed some light on the more complex relationships in this unit. I also propose mapping the BRUMC exposures north of the BRF. My field work focused on the mélange exposures and I only sampled the rocks north of the BRF to provide some missing age constraints from this part of the arc. However, I noticed that there was substantial variation in the BRUMC exposures just north of the BRF on a reconnaissance sampling day. This area has never

been mapped in detail before, and it may shed some light on the system of faults that make up the BRF.

Finally, fractures and faults are pervasive throughout the McHugh Complex, the southern BRUMC, and the Valdez Group. If these structures could be measured and mapped at sufficient density, this well-exposed part of the McHugh Complex could lead to a better understanding of the low-temperature deformation histories of these three exposures, if the facture patterns and densities are similar or different.

References

Amato, J.M., and Pavlis, T.L. 2010. Detrital zircon ages from the Chugach terrane, southern Alaska, reveal multiple episodes of accretion and erosion in a subduction complex. Geology, **38**: 459–462. doi:10.1130/G30719.1.

Amato, J.M., Pavlis, T.L., Clift, P.D., Kochelek, E.J., Hecker, J.P., Worthman, C.M., and Day, E.M. 2013. Architecture of the Chugach accretionary complex as revealed by detrital zircon ages and lithologic variations: Evidence for Mesozoic subduction erosion in south-central Alaska. Bulletin of the Geological Society of America, **125**: 1891–1911. doi:10.1130/B30818.1.

Bradley, D.C., Haeussler, P.J., and Kusky, T.M. 1993. Timing of early Tertiary ridge subduction in southern Alaska. U.S. Geological Survey Bulletin 2068: 163-177.

Burns, L.E., Pessel, G.H., Little, T.A., Pavlis, T.L., Newberry, R.J., Winkler, G.R., and Decker, J. 1991. Geology of the northern Chugach Mountains, southcentral Alaska. Alaska Division of Geological and Geophysical Surveys Professional Report 94.

Clark, S.H.B. 1973. The McHugh Complex of south-central Alaska. U.S. Geological Survey Bulletin 1372-D.

Cowan, D.S. 1985. Structural styles in Mesozoic and Cenozoic mélanges in the western Cordillera of North America. Geological Society of America Bulletin, **96**: 451–462. doi:10.1130/0016-7606(1985)96<451:SSIMAC>2.0.CO;2.

Garver, J.I., and Davidson, C.M. 2015. Southwestern Laurentian zircons in Upper Cretaceous flysch of the Chugach-Prince William terrane in Alaska. American Journal of Science, **315**: 537-556. doi:10.2475/06.2015.02.

Lytwyn, J., Lockhart, S., Casey, J., and Kusky, T. 2000. Geochemistry of near-trench intrusives associated with ridge subduction, Seldovia Quadrangle, southern Alaska. Journal of Geophysical Research, **105**: 27957-27978.

Wakabayashi, J. 2015. Anatomy of a subduction complex: architecture of the Franciscan Complex, California, at multiple length and time scales. International Geology Review, **57**: 669-746. doi:10.1080/00206814.2014.998728.

Appendix A: Geochronological Data

Presented below are the geochronological data from zircon U-Pb analyses from the University of British Columbia and the University of New Brunswick. Also presented are the $^{40}Ar/^{39}Ar$ data from the University of Manitoba. A concordia diagram for zircon U-Pb analyses for sample 16Ba03 was omitted from the above manuscript and follows the data tables.

Figure A.1 shows zircon analyses from sample 16Ba03, a trachyandesite from a decapitated seamount incorporated into the McHugh Complex at the base of Nelchina Glacier. These ages are spread across concordia and some ages are younger than the McHugh Complex, which is Jurassic to mid-Cretaceous in age. The younger ages are considered to be contamination from the separation lab, or the analytical lab. This also implies that there could be contamination among the zircon population older than the McHugh Complex. The older population could also be detrital, which would mean that the lavas that formed these pillows flowed over sea-floor sediment as it was extruded. Some zircons show what may be a discordia curve from ~2.5 Ga to ~500 Ma. This could mean that ~2.5 Ga zircons suffered a partial resetting event at ~500 Ma and then were incorporated into this trachyandesite. Another, unfavored interpretation, is that the seamount itself is 2.5 Ga. This is far older than any known ocean crust is known to be able to reach.

Table A.1: Zircon isotopic U-Pb data for samples 16Ba02, 16Ba21, and 16Ba03. Weighted mean ages for samples 16Ba02 and 16Ba21 based on $^{206}Pb/^{238}U$ single zircon ages. Sample 16Ba03 did not yield a meaningful weighted mean age.

		Isotopic Ratios							Apparent Ages (Ma)					
	U* (ppm)	$^{207}Pb/^{235}U$	2σ (abs)	$^{206}Pb/^{238}U$	2σ (abs)	ρ	$^{207}Pb/^{206}Pb$	2σ (abs)	$^{207}Pb/^{235}U$	2σ	$^{206}Pb/^{238}U$	2σ	$^{207}Pb/^{206}Pb$	2σ
16Ba02-1		0.056	0.014	0.0088	0.0007	0.0161	0.074	0.019	52.0	13.0	56.2	4.6	-360	330
16Ba02-2		0.049	0.016	0.0080	0.0008	0.2271	0.300	1.200	44.0	14.0	51.0	5.1		
16Ba02-3		0.056	0.014	0.0082	0.0007	0.0263	0.180	0.210	52.0	13.0	52.5	4.6	130	610
16Ba02-4		0.055	0.011	0.0082	0.0005	0.0426	0.050	0.007	53.0	10.0	52.5	3.5	-40	210
16Ba02-5		0.060	0.013	0.0080	0.0006	0.0514	0.081	0.022	57.0	13.0	51.4	4.1	-30	320
16Ba02-6		0.059	0.014	0.0087	0.0007	0.0713	0.069	0.017	56.0	13.0	56.0	4.7	-240	310
16Ba02-7		0.059	0.010	0.0080	0.0005	0.0204	0.061	0.007	57.6	9.8	51.5	3.3	260	180
16Ba02-8		0.053	0.010	0.0081	0.0005	0.1192	0.048	0.006	51.4	9.3	51.9	3.3	-10	180
16Ba02-9		0.057	0.011	0.0083	0.0006	0.0517	0.075	0.018	55.0	11.0	53.5	4.1	170	250
16Ba02-10		0.064	0.015	0.0081	0.0007	0.1314	0.087	0.026	60.0	14.0	52.2	4.5	130	330
16Ba02-11		0.076	0.021	0.0089	0.0010	0.0799	0.570	0.540	70.0	19.0	57.0	6.6		
16Ba02-12		0.053	0.010	0.0082	0.0006	0.0509	0.053	0.008	51.3	9.3	52.4	3.8	80	220
16Ba02-13		0.053	0.015	0.0082	0.0008	0.0503	-1.000	1.400	48.0	14.0	52.5	5.0		
16Ba02-14		0.047	0.011	0.0081	0.0006	0.0744	0.070	0.014	45.0	10.0	52.2	3.9	150	450
16Ba02-15		0.050	0.012	0.0081	0.0006	0.0701	0.061	0.014	48.0	11.0	52.2	3.9	-40	270
16Ba02-16		0.065	0.012	0.0086	0.0006	0.0666	0.055	0.008	63.0	12.0	55.3	4.0	130	250
16Ba02-17		0.058	0.012	0.0086	0.0007	0.0259	0.069	0.013	55.0	11.0	55.4	4.2	80	240
16Ba02-18		0.055	0.015	0.0084	0.0007	0.0261	0.079	0.023	51.0	14.0	53.9	4.7	-220	340
16Ba02-19		0.051	0.012	0.0080	0.0006	0.0056	0.056	0.010	47.0	11.0	51.6	3.8	-210	240
16Ba02-20		0.058	0.013	0.0086	0.0007	0.0775	0.073	0.016	55.0	12.0	55.0	4.7	210	540
									Weighted mean $^{206}Pb/^{238}U$ age – 53.04 ± 0.94 Ma					
16Ba21-1		0.225	0.013	0.0302	0.0011	0.1828	0.054	0.004	207.0	12.0	191.9	6.9	340	140
16Ba21-2		0.214	0.012	0.0294	0.0008	0.2138	0.052	0.003	195.3	9.8	186.8	5.0	240	130
16Ba21-3		0.109	0.004	0.0160	0.0003	0.2432	0.049	0.002	105.1	3.4	102.5	2.1	172	91
16Ba21-4		0.080	0.004	0.0120	0.0003	0.1869	0.049	0.003	77.6	3.6	76.9	1.9	140	110
16Ba21-5		0.208	0.009	0.0307	0.0008	0.3403	0.049	0.003	190.8	7.8	194.7	4.9	180	110
16Ba21-6		0.205	0.010	0.0304	0.0008	0.1487	0.051	0.003	191.3	8.7	192.8	4.8	230	120
16Ba21-7		0.215	0.011	0.0306	0.0009	0.2824	0.051	0.003	196.7	8.9	194.1	5.4	200	120
16Ba21-8		0.207	0.006	0.0301	0.0006	0.3209	0.050	0.002	190.7	5.2	191.0	4.0	199	91
16Ba21-9		0.212	0.010	0.0299	0.0008	0.3028	0.052	0.003	194.8	8.7	189.9	4.8	270	120
16Ba21-10		0.075	0.003	0.0111	0.0003	0.2186	0.049	0.003	73.9	3.1	71.3	1.6	170	100
16Ba21-11		0.222	0.016	0.0311	0.0012	0.0320	0.051	0.004	202.0	13.0	197.5	7.3	270	160
16Ba21-12		0.199	0.010	0.0292	0.0009	0.0412	0.050	0.004	183.6	8.6	185.4	5.4	200	140
16Ba21-13		0.212	0.010	0.0301	0.0009	0.4970	0.051	0.003	194.4	8.7	190.8	5.8	210	110
16Ba21-14		0.213	0.009	0.0289	0.0008	0.2290	0.052	0.003	195.9	7.0	183.3	5.2	290	110
16Ba21-15		0.213	0.018	0.0291	0.0011	0.1510	0.052	0.005	197.0	15.0	185.1	7.0	230	170
16Ba21-16		0.210	0.013	0.0289	0.0010	0.2240	0.051	0.004	192.0	11.0	183.4	6.2	210	130
16Ba21-17		0.209	0.015	0.0296	0.0009	0.0626	0.049	0.004	191.0	12.0	188.0	5.8	130	150
16Ba21-18		0.078	0.003	0.0110	0.0004	0.4580	0.050	0.003	75.8	3.0	70.5	2.6	190	110
16Ba21-19		0.212	0.009	0.0295	0.0007	0.1863	0.051	0.003	194.0	7.8	187.3	4.7	220	110
16Ba21-20		0.209	0.008	0.0289	0.0007	0.2299	0.051	0.003	192.6	7.1	183.5	4.3	250	100
									Weighted mean $^{206}Pb/^{238}U$ age – 188.9 ± 2.2 Ma					

(continued)

16Ba03-1	44	0.503	0.020	0.0643	0.0012	0.1639	0.056	0.002	412	14	401.4	7.3	455	75
16Ba03-2	204	15.0	0.390	0.5382	0.0100	0.5599	0.203	0.003	2812	25	2774	43	2846	25
16Ba03-3	260	14.6	0.550	0.5300	0.0160	0.6539	0.201	0.005	2787	36	2739	65	2837	41
16Ba03-4	112	5.53	0.120	0.3436	0.0058	0.7926	0.117	0.001	1906.8	19	1903	28	1915	16
16Ba03-5	382	0.085	0.010	0.0099	0.0004	0.2696	0.062	0.008	81.9	9.3	63.2	2.6	560	260
16Ba03-6	210	12.5	0.360	0.4835	0.0091	0.5355	0.188	0.003	2640	27	2541	40	2714	30
16Ba03-7	401	0.103	0.013	0.0125	0.0005	0.0488	0.062	0.008	98	12	79.9	3	490	250
16Ba03-8	111	4.87	0.130	0.3121	0.0052	0.4519	0.114	0.002	1795	22	1751	25	1852	30
16Ba03-9	171	0.020	0.004	0.0007	0.0001	0.1847	0.208	0.044	19.8	4.1	4.7	0.36	1620	550
16Ba03-10	353	10.9	0.400	0.3570	0.0110	0.8237	0.222	0.004	2505	33	1964	53	2993	29
16Ba03-11	125	13.7	0.750	0.4300	0.0220	0.8593	0.230	0.006	2716	53	2300	99	3047	42
16Ba03-12	340	0.501	0.019	0.0612	0.0011	0.2643	0.059	0.002	411	13	383.8	6.9	561	66
16Ba03-13	388	1.66	0.055	0.1611	0.0029	0.1664	0.075	0.002	991	22	963	16	1076	51
16Ba03-14	220	0.523	0.043	0.0046	0.0004	0.6833	0.866	0.050	420	28	29.2	2.4	5110	110
16Ba03-15	40	3.29	0.120	0.1219	0.0043	0.7962	0.196	0.004	1477	29	741	25	2788	34
16Ba03-16	54	11.4	0.270	0.4388	0.0079	0.7782	0.189	0.002	2554	22	2344	35	2729	16
16Ba03-17	498	3.00	0.087	0.2367	0.0041	0.4788	0.092	0.002	1404	22	1369	22	1465	37
16Ba03-18	70	12.8	0.370	0.4962	0.0100	0.5318	0.187	0.004	2661	27	2596	44	2707	31
16Ba03-19	596	0.044	0.006	0.0057	0.0002	0.0605	0.057	0.008	43.4	5.8	36.4	1.3	260	230
16Ba03-20	43	11.2	0.310	0.4575	0.0100	0.6508	0.180	0.003	2539	28	2426	44	2643	31
16Ba03-21	151	0.603	0.032	0.0469	0.0009	0.0514	0.094	0.005	478	20	295.7	5.3	1475	95
16Ba03-22	109	4.67	0.180	0.3002	0.0067	0.3728	0.113	0.004	1757	33	1692	33	1828	60
16Ba03-23	99	10.5	0.250	0.4577	0.0079	0.5317	0.168	0.002	2480	22	2429	35	2532	22
16Ba03-24	1168	2.04	0.059	0.1893	0.0031	0.3313	0.079	0.002	1125	20	1117	17	1151	45
16Ba03-25	37	10.1	1.700	0.4220	0.0140	0.6263	0.173	0.015	2370	170	2262	63	2590	140
16Ba03-26	113	0.362	0.018	0.0461	0.0010	0.0931	0.058	0.003	313	13	290.3	6.2	480	100
16Ba03-27	231	1.96	0.056	0.1715	0.0027	0.1661	0.083	0.002	1101	19	1019.9	15	1260	43
16Ba03-28	43	12.8	0.380	0.4736	0.0090	0.5385	0.197	0.004	2665	28	2498	39	2800	30
16Ba03-29	147	13.5	0.320	0.5199	0.0082	0.6962	0.188	0.002	2712	22	2698	35	2724	17
16Ba03-30	102	4.96	0.130	0.3166	0.0053	0.5702	0.114	0.002	1814	24	1772	26	1858	29
16Ba03-31	180	0.031	0.009	0.0005	0.0001	0.0397	0.000	0.540	30.7	9	3.21	0.82	-7100	7800
16Ba03-32	137	12.2	0.340	0.4748	0.0100	0.5503	0.188	0.003	2619	26	2502	44	2714	30
16Ba03-33	63	4.09	0.110	0.2844	0.0047	0.4914	0.105	0.002	1652	24	1613	23	1701	34
16Ba03-34	70	11.2	1.200	0.4440	0.0120	0.5437	0.180	0.014	2512	110	2368	55	2600	140
16Ba03-35	41	9.88	0.630	0.3370	0.0210	0.8890	0.211	0.003	2407	58	1861	100	2911	25
16Ba03-36	34	11.5	0.430	0.4090	0.0140	0.5452	0.207	0.006	2563	34	2209	62	2869	48
16Ba03-37	290	0.228	0.027	0.0228	0.0008	0.1447	0.073	0.009	203	22	145.6	5.1	720	230
16Ba03-38	112	16.0	0.480	0.5363	0.0110	0.6654	0.216	0.004	2868	29	2765	45	2943	28
16Ba03-39	410	0.007	0.004	0.0002	0.0000	0.0720	-0.180	0.310	7.2	4.2	1.11	0.3	-18900	9800
16Ba03-40	507	0.801	0.042	0.0944	0.0021	0.2278	0.062	0.003	591	24	581.1	12	590	110
16Ba03-41	98	9.75	0.420	0.3859	0.0100	0.8406	0.182	0.004	2401	41	2100	47	2667	37
16Ba03-42	210	0.309	0.015	0.0440	0.0008	0.1930	0.051	0.002	273	11	277.8	5.1	217	88
16Ba03-43	28	12.2	0.380	0.4560	0.0120	0.6341	0.194	0.004	2618	29	2421	54	2769	35
16Ba03-44	159	4.06	0.120	0.2735	0.0052	0.6088	0.107	0.002	1643	23	1558	26	1745	31
16Ba03-45	55	3.39	0.610	0.1390	0.0120	0.7244	0.161	0.025	1380	150	829	65	2640	180
16Ba03-46	62	12.6	0.360	0.4947	0.0120	0.6826	0.185	0.003	2650	27	2589	50	2692	27
16Ba03-47	37	13.0	0.330	0.5119	0.0100	0.5185	0.185	0.003	2678	25	2662	44	2691	27
16Ba03-48	1062	14.5	0.370	0.5095	0.0091	0.7185	0.207	0.003	2780	24	2653	39	2875	21
16Ba03-49	83	13.3	0.360	0.4893	0.0093	0.4810	0.196	0.004	2694	26	2566	40	2789	30
16Ba03-50	193	0.494	0.019	0.0641	0.0010	0.1290	0.056	0.002	406	13	400.6	6.2	416	70
16Ba03-51	3770	1.73	0.054	0.1691	0.0027	0.3405	0.074	0.002	1018	19	1007.2	15	1026	46
16Ba03-52	41400	1.77	0.057	0.1689	0.0031	0.4576	0.075	0.002	1030	21	1006	17	1065	48
16Ba03-53	125	8.19	0.240	0.3725	0.0069	0.8824	0.159	0.002	2248	27	2040	32	2445	21
16Ba03-54	22	18.0	1.500	0.4990	0.0180	0.8239	0.255	0.013	2932	72	2612	77	3155	79
16Ba03-55	0	12.8	0.500	0.4550	0.0120	0.7958	0.203	0.005	2661	38	2415	53	2847	37
16Ba03-56	0	27.9	2.400	0.6060	0.0230	0.7521	0.328	0.018	3391	96	3047	94	3584	92

NOTE: Samples 16Ba02 and 16Ba21 analyzed at the University of British Columbia. Sample 16Ba03 analyzed at the University of New Brunswick.

Table A.2: Amphibole $^{40}Ar/^{39}Ar$ isotopic data for samples 16Ba21 and 16Ba28.

Laser Power (%)	Relative Isotopic abundances (fAmps)* ^{40}Ar	± (1σ)	^{39}Ar	± (1σ)	^{38}Ar	± (1σ)	^{37}Ar	± (1σ)	^{36}Ar	± (1σ)	Ca/K	± (1σ)	Cl/K	± (1σ)	$^{40}Ar^*/^{39}Ar_{(K)}$	± (1σ)	$^{40}Ar^*$ (%)	Age (Ma)	± (1σ)
Sample 16Ba21, BRUMC, amphibole, J = 0.002699 ± 1.63E-06																			
Aliquot 1																			
0.5	14.770	0.0621	-0.0622	0.0620	-0.0124	0.0290	0.1978	0.0254	0.0490	0.0014	-20.194	20.810	0.965	1.692	-5.389	8.633	2.286	-26.4	42.7
2	69.753	0.0723	1.2019	0.0601	0.0353	0.0283	10.1218	0.0286	0.0792	0.0017	54.939	2.901	0.017	0.071	41.498	2.230	70.166	191.5	9.8
2.5	365.734	0.0946	9.0570	0.0619	0.0716	0.0318	30.6625	0.0277	0.0621	0.0015	21.845	0.169	-0.015	0.010	39.507	0.288	97.125	182.8	1.3
3	373.695	0.0841	9.3462	0.0661	0.1541	0.0291	29.2041	0.0312	0.0524	0.0015	20.178	0.161	0.011	0.009	39.391	0.297	97.860	182.3	1.3
4	80.613	0.0687	1.9759	0.0635	-0.0615	0.0312	7.4983	0.0302	0.0180	0.0012	24.576	0.832	-0.130	0.047	39.405	1.332	95.794	182.4	5.9
5	63.669	0.0725	1.5897	0.0646	0.0836	0.0293	6.0194	0.0283	0.0088	0.0012	24.537	1.048	0.116	0.055	39.721	1.699	98.366	183.7	7.5
Aliquot 2																			
0.5	1.256	0.0604	0.0512	0.0624	-0.0105	0.0291	0.0325	0.0252	0.0042	0.0009	4.085	6.070	-0.673	1.886	0.237	5.361	0.967	1.2	26.1
2	57.160	0.0720	1.1088	0.0667	0.0026	0.0297	4.1105	0.0278	0.0676	0.0016	24.067	1.519	-0.061	0.080	34.759	2.223	66.885	161.8	9.9
2.25	124.348	0.0820	3.1116	0.0668	0.0848	0.0304	10.4288	0.0262	0.0242	0.0012	21.755	0.494	0.041	0.029	38.808	0.876	96.410	179.7	3.9
2.5	359.939	0.0859	9.1534	0.0619	0.1595	0.0301	28.6824	0.0302	0.0399	0.0014	20.357	0.156	0.014	0.010	39.105	0.282	98.777	181.0	1.2
2.75	198.522	0.0855	5.0225	0.0571	0.0382	0.0308	15.6619	0.0271	0.0249	0.0011	20.271	0.249	-0.015	0.018	39.129	0.470	98.331	181.1	2.1
3	19.231	0.0592	0.5027	0.0621	-0.0225	0.0286	1.6613	0.0252	0.0017	0.0010	21.506	2.785	-0.167	0.171	38.405	4.972	99.677	178.0	21.9
4	130.156	0.0798	3.2422	0.0580	0.0869	0.0300	12.4251	0.0271	0.0203	0.0011	25.004	0.475	0.041	0.028	39.619	0.748	97.868	183.3	3.3
5	14.261	0.0622	0.4153	0.0621	-0.0613	0.0297	1.5099	0.0273	0.0016	0.0009	23.723	3.724	-0.468	0.226	34.411	5.405	99.429	160.2	24.1
Sample 16Ba28, BRUMC, amphibole, J = 0.002699 ± 1.5E-06																			
Aliquot 1																			
0.5	1.526	0.0592	0.0125	0.0011	-0.0383	0.0372	0.0915	0.0331	0.0037	0.0009	47.386	17.872	-9.258	9.004	36.500	23.217	29.354	169.5	102.9
2	72.323	0.0666	0.5933	0.0678	0.0998	0.0234	3.1042	0.0227	0.2060	0.0023	33.663	4.019	0.269	0.122	20.847	2.772	16.906	98.7	12.8
2.5	80.430	0.0717	2.1531	0.0642	0.0474	0.0301	29.0903	0.0315	0.1129	0.0020	88.659	2.828	0.005	0.043	26.073	0.879	67.700	122.7	4.0
3	141.305	0.0769	3.8741	0.0634	0.1531	0.0306	44.5908	0.0310	0.1370	0.0020	75.283	1.328	0.066	0.024	29.718	0.542	79.391	139.2	2.4
4	32.525	0.0722	0.9724	0.0623	-0.0387	0.0310	14.1964	0.0278	0.0367	0.0013	96.238	6.585	-0.172	0.098	26.886	1.887	77.766	126.4	8.6
5	23.184	0.0676	0.8646	0.0631	0.1208	0.0269	11.9164	0.0281	0.0237	0.0013	90.749	7.051	0.372	0.099	22.954	1.838	82.965	108.4	8.4
Aliquot 2																			
2	275.596	0.0948	5.0998	0.0605	0.1381	0.0311	15.5104	0.0278	0.2939	0.0027	22.189	0.282	0.013	0.018	38.169	0.504	70.113	176.9	2.2
2.5	382.968	0.1018	8.9186	0.0666	0.1853	0.0309	26.3917	0.0310	0.1660	0.0021	21.599	0.178	0.016	0.010	38.572	0.311	89.188	178.7	1.4
2.8	328.255	0.0895	7.0569	0.0634	0.1184	0.0296	20.4718	0.0289	0.1918	0.0024	21.185	0.207	0.000	0.013	39.599	0.387	84.538	183.2	1.7
3	463.860	0.1063	9.9534	0.0622	0.2277	0.0310	30.2620	0.0286	0.2660	0.0027	22.241	0.156	0.018	0.009	39.881	0.277	84.948	184.4	1.2
4	410.818	0.1073	1.5109	0.0584	0.2472	0.0286	5.4553	0.0283	1.1901	0.0054	26.470	1.077	0.012	0.057	40.555	2.088	14.784	187.4	9.2
5	41.343	0.0587	0.1277	0.0616	-0.0130	0.0311	0.4945	0.0259	0.1244	0.0020	28.434	14.377	-0.867	0.848	37.394	19.397	11.438	173.5	85.8

* Corrected for blank, mass discrimination, and radioactive decay

Sensitivity 6.312E-17 ± 1.047E-18 (mol/fAmp)

Table A.3: Whole-rock $^{40}Ar/^{39}Ar$ isotopic data for samples 150715-12 and 16Ba03.

Laser Power (%)	Relative Isotopic abundances (fAmps)* ^{40}Ar	± (1σ)	^{39}Ar	± (1σ)	^{38}Ar	± (1σ)	^{37}Ar	± (1σ)	^{36}Ar	± (1σ)	Ca/K	± (1σ)	Cl/K	± (1σ)	$^{40}Ar^*/^{39}Ar_{(K)}$	± (1σ)	$^{40}Ar^*$ (%)	Age (Ma)	± (1σ)
Sample 150715-12, pillow trachybasalt, whole-rock, J = 0.002704 ± 2.49E-06																			
Aliquot 1																			
0.5	14.737	0.0665	1.1814	0.0632	-0.0092	0.0322	0.4411	0.0280	0.0131	0.0012	2.303	0.195	-0.064	0.081	9.291	0.604	74.462	44.8	2.9
0.8	20.641	0.0673	1.7424	0.0658	0.0439	0.0297	0.5687	0.0265	0.0140	0.0012	2.015	0.123	0.033	0.050	9.552	0.428	80.619	46.0	2.0
1	42.978	0.0663	3.4338	0.0636	0.0505	0.0332	0.6273	0.0270	0.0109	0.0013	1.128	0.054	0.006	0.029	11.620	0.248	92.850	55.8	1.2
1.4	108.722	0.0799	7.7082	0.0642	0.1114	0.0301	1.3326	0.0272	0.0261	0.0014	1.069	0.024	0.005	0.012	13.144	0.127	93.200	63.0	0.6
1.7	151.391	0.0807	8.8850	0.0683	0.1241	0.0280	1.7016	0.0265	0.0123	0.0011	1.185	0.021	0.004	0.009	16.678	0.139	97.887	79.6	0.6
2	99.616	0.0760	6.1666	0.0600	0.0459	0.0299	1.4922	0.0257	0.0053	0.0011	1.498	0.030	-0.014	0.014	15.959	0.170	98.787	76.2	0.8
2.25	71.415	0.0676	5.1614	0.0657	0.0309	0.0319	1.5995	0.0264	0.0028	0.0012	1.922	0.041	-0.018	0.018	13.755	0.194	99.389	65.9	0.9
2.5	50.134	0.0725	3.8738	0.0613	0.1011	0.0309	1.7788	0.0282	0.0064	0.0011	2.851	0.066	0.040	0.024	12.575	0.223	97.114	60.3	1.1
2.75	41.773	0.0646	3.0078	0.0576	-0.0458	0.0302	1.6375	0.0289	0.0217	0.0012	3.383	0.091	-0.083	0.030	11.899	0.264	85.619	57.1	1.2
3	46.751	0.0694	3.7253	0.0652	0.0076	0.0281	3.3943	0.0258	0.0076	0.0010	5.673	0.113	-0.030	0.022	12.191	0.237	96.991	58.5	1.1
4	116.355	0.0726	9.1992	0.0597	0.0790	0.0301	12.0375	0.0282	0.0368	0.0012	8.161	0.063	-0.012	0.010	11.821	0.090	93.234	56.8	0.4
5	25.915	0.0664	2.0121	0.0608	-0.0459	0.0327	1.4553	0.0292	0.0078	0.0009	4.508	0.168	-0.104	0.048	11.919	0.399	92.442	57.2	1.9
6	9.122	0.0661	0.5583	0.0615	-0.0149	0.0290	0.5412	0.0280	-0.0031	0.0009	6.053	0.758	-0.110	0.155	18.225	2.135	111.363	86.8	9.9
7	10.288	0.0640	0.7481	0.0621	-0.0062	0.0284	0.5306	0.0289	0.0017	0.0009	4.429	0.452	-0.061	0.113	13.253	1.199	96.269	63.5	5.6
Sample 16Ba03, pillow trachyandesite, whole-rock, J = 0.002703 ± 2.36E-06																			
Aliquot 1																			
0.5	466.202	0.1110	43.6051	0.0633	0.5579	0.0284	0.3727	0.0277	0.0450	0.0013	0.053	0.004	0.001	0.002	10.384	0.018	97.168	49.9	0.1
0.8	172.120	0.0776	15.2437	0.0686	0.1577	0.0281	0.1273	0.0298	0.0032	0.0010	0.052	0.012	-0.005	0.005	11.226	0.056	99.472	53.9	0.3
1	236.835	0.0897	19.0335	0.0630	0.1881	0.0334	0.1145	0.0281	0.0054	0.0010	0.037	0.009	-0.007	0.005	12.354	0.045	99.332	59.3	0.2
1.4	430.292	0.1045	32.6421	0.0627	0.3475	0.0292	0.2339	0.0261	0.0081	0.0011	0.044	0.005	-0.005	0.003	13.104	0.028	99.456	62.8	0.1
1.7	381.962	0.0942	28.2807	0.0622	0.3446	0.0296	0.2222	0.0290	0.0123	0.0010	0.049	0.007	0.000	0.003	13.374	0.033	99.065	64.1	0.2
2	494.698	0.1196	37.3085	0.0663	0.4350	0.0296	0.2864	0.0278	0.0155	0.0011	0.048	0.005	-0.002	0.002	13.133	0.026	99.087	62.9	0.1
2.25	465.359	0.1067	35.2804	0.0646	0.3659	0.0348	0.2582	0.0262	0.0193	0.0012	0.046	0.005	-0.006	0.003	13.024	0.027	98.787	62.4	0.1
2.5	403.632	0.0939	29.8784	0.0672	0.4752	0.0302	0.2804	0.0272	0.0162	0.0011	0.059	0.006	0.010	0.003	13.346	0.033	98.834	63.9	0.2
2.75	297.975	0.0944	21.1193	0.0674	0.2416	0.0290	0.2038	0.0264	0.0114	0.0011	0.060	0.008	-0.003	0.004	13.946	0.049	98.890	66.7	0.2
3	171.736	0.0845	11.6935	0.0658	0.1215	0.0292	0.1048	0.0285	0.0069	0.0010	0.056	0.016	-0.006	0.007	14.508	0.088	98.831	69.4	0.4
4	275.694	0.0938	17.3629	0.0618	0.2482	0.0284	0.0830	0.0276	0.0252	0.0012	0.030	0.010	0.005	0.005	15.444	0.061	97.307	73.8	0.3
5	98.550	0.0737	5.9691	0.0617	0.1020	0.0302	0.1377	0.0271	0.0302	0.0012	0.145	0.029	0.011	0.015	15.016	0.172	90.988	71.8	0.8
6	130.887	0.0782	8.0544	0.0651	0.1318	0.0293	0.1385	0.0282	0.0366	0.0012	0.108	0.022	0.010	0.011	14.906	0.132	91.766	71.3	0.6
7	106.917	0.0742	6.9298	0.0635	0.1160	0.0304	0.2522	0.0254	0.0355	0.0012	0.230	0.023	0.010	0.013	13.921	0.142	90.261	66.6	0.7
Aliquot 2																			
0.5	112.472	0.0733	15.2692	0.0650	0.2109	0.0318	0.1047	0.0274	0.0991	0.0017	0.048	0.013	0.001	0.006	5.446	0.043	73.974	26.4	0.2
0.8	519.673	0.1022	51.6158	0.0678	0.6821	0.0316	0.4414	0.0268	0.1286	0.0021	0.060	0.004	0.002	0.002	9.329	0.020	92.708	44.9	0.1
1	579.744	0.1104	45.4191	0.0630	0.5110	0.0327	0.2687	0.0256	0.0761	0.0018	0.041	0.004	-0.004	0.002	12.265	0.024	96.134	58.8	0.1
1.4	773.222	0.1036	57.4677	0.0481	0.6141	0.0202	0.3232	0.0182	0.0783	0.0014	0.039	0.002	-0.005	0.001	13.047	0.017	97.019	62.5	0.1
1.7	825.380	0.1275	64.0003	0.0697	0.7239	0.0329	0.4402	0.0283	0.0535	0.0014	0.048	0.003	-0.003	0.002	12.645	0.019	98.100	60.6	0.1
2	867.969	0.1463	67.4562	0.0708	0.7662	0.0300	0.5497	0.0259	0.0828	0.0018	0.057	0.003	-0.003	0.001	12.500	0.019	97.197	59.9	0.1
2.25	755.166	0.1307	55.5426	0.0695	0.5641	0.0311	0.4411	0.0296	0.0966	0.0018	0.056	0.004	-0.007	0.002	13.078	0.023	96.235	62.7	0.1
2.5	306.286	0.0929	20.9037	0.0726	0.2223	0.0265	0.2025	0.0255	0.0332	0.0013	0.068	0.009	-0.005	0.004	14.178	0.056	96.814	67.8	0.3
2.75	148.415	0.0778	9.7205	0.0626	0.0687	0.0311	0.1054	0.0291	0.0102	0.0010	0.076	0.021	-0.015	0.009	14.953	0.105	97.983	71.5	0.5
3	24.765	0.0639	1.6412	0.0664	0.0707	0.0285	-0.0561	0.0283	0.0001	0.0010	-0.243	0.124	0.089	0.051	15.063	0.655	99.881	72.0	3.1

(continued)

4	230.583	0.0952	14.9951	0.0641	0.1514	0.0311	0.0848	0.0271	0.0244	0.0011	0.040	0.013	-0.007	0.006	14.890	0.071	96.877	71.2	0.3
5	132.427	0.0765	9.2348	0.0617	0.1070	0.0305	0.1321	0.0277	0.0188	0.0011	0.101	0.022	-0.003	0.010	13.734	0.103	95.823	65.8	0.5
6	130.813	0.0746	9.5294	0.0620	0.1138	0.0279	0.1135	0.0260	0.0197	0.0012	0.084	0.020	-0.002	0.009	13.114	0.096	95.579	62.8	0.5
7	84.428	0.0728	5.6776	0.0613	0.0095	0.0277	0.0716	0.0271	0.0081	0.0010	0.089	0.034	-0.031	0.014	14.447	0.170	97.198	69.1	0.8
Aliquot 3																			
0.5	217.052	0.0906	17.5300	0.0625	0.2951	0.0323	0.1137	0.0298	0.1737	0.0025	0.046	0.012	0.008	0.005	9.451	0.057	76.369	45.5	0.3
0.8	147.959	0.0798	13.7772	0.0646	0.0769	0.0291	0.0635	0.0283	0.0087	0.0012	0.032	0.015	-0.020	0.006	10.548	0.058	98.272	50.7	0.3
1	301.996	0.0898	23.7376	0.0619	0.1908	0.0290	0.0795	0.0286	0.0214	0.0012	0.023	0.009	-0.013	0.004	12.450	0.038	97.913	59.7	0.2
1.2	353.930	0.1016	24.8680	0.0629	0.2486	0.0315	0.0762	0.0272	0.0287	0.0014	0.021	0.008	-0.007	0.004	13.885	0.042	97.611	66.5	0.2
1.4	831.734	0.1278	56.6103	0.0691	0.6329	0.0301	0.2530	0.0257	0.0638	0.0015	0.032	0.003	-0.004	0.002	14.353	0.023	97.741	68.7	0.1
1.6	795.026	0.1242	58.9307	0.0686	0.7007	0.0304	0.3158	0.0264	0.0471	0.0015	0.038	0.003	-0.001	0.002	13.250	0.021	98.261	63.5	0.1
1.8	731.620	0.1183	56.9158	0.0648	0.7090	0.0301	0.3492	0.0278	0.0556	0.0015	0.044	0.004	0.000	0.002	12.561	0.020	97.766	60.2	0.1
2	888.188	0.1384	69.1702	0.0707	0.8297	0.0324	0.4935	0.0295	0.0775	0.0019	0.051	0.003	-0.001	0.001	12.505	0.019	97.438	60.0	0.1
2.2	743.226	0.1309	56.3588	0.0641	0.6699	0.0318	0.3942	0.0264	0.0502	0.0015	0.050	0.003	-0.001	0.002	12.919	0.020	98.018	61.9	0.1
2.4	495.049	0.1106	36.5039	0.0621	0.4744	0.0321	0.2177	0.0246	0.0301	0.0013	0.042	0.005	0.002	0.003	13.313	0.028	98.216	63.8	0.1
2.6	493.895	0.0993	35.7935	0.0664	0.4767	0.0348	0.2921	0.0248	0.0267	0.0013	0.058	0.005	0.003	0.003	13.573	0.030	98.418	65.0	0.1
3	367.219	0.0986	26.3119	0.0646	0.2319	0.0285	0.1839	0.0279	0.0166	0.0011	0.050	0.008	-0.010	0.003	13.765	0.039	98.678	65.9	0.2
4	478.744	0.1093	33.0128	0.0598	0.3528	0.0288	0.2022	0.0296	0.0374	0.0013	0.044	0.007	-0.005	0.003	14.161	0.031	97.700	67.8	0.1
6	503.765	0.1021	36.2063	0.0734	0.4448	0.0288	0.3557	0.0259	0.0730	0.0018	0.071	0.005	-0.001	0.002	13.314	0.034	95.737	63.8	0.2

* Corrected for blank, mass discrimination, and radioactive decay

Sensitivity 6.312E-17 ± 1.047E-18 (mol/fAmp)

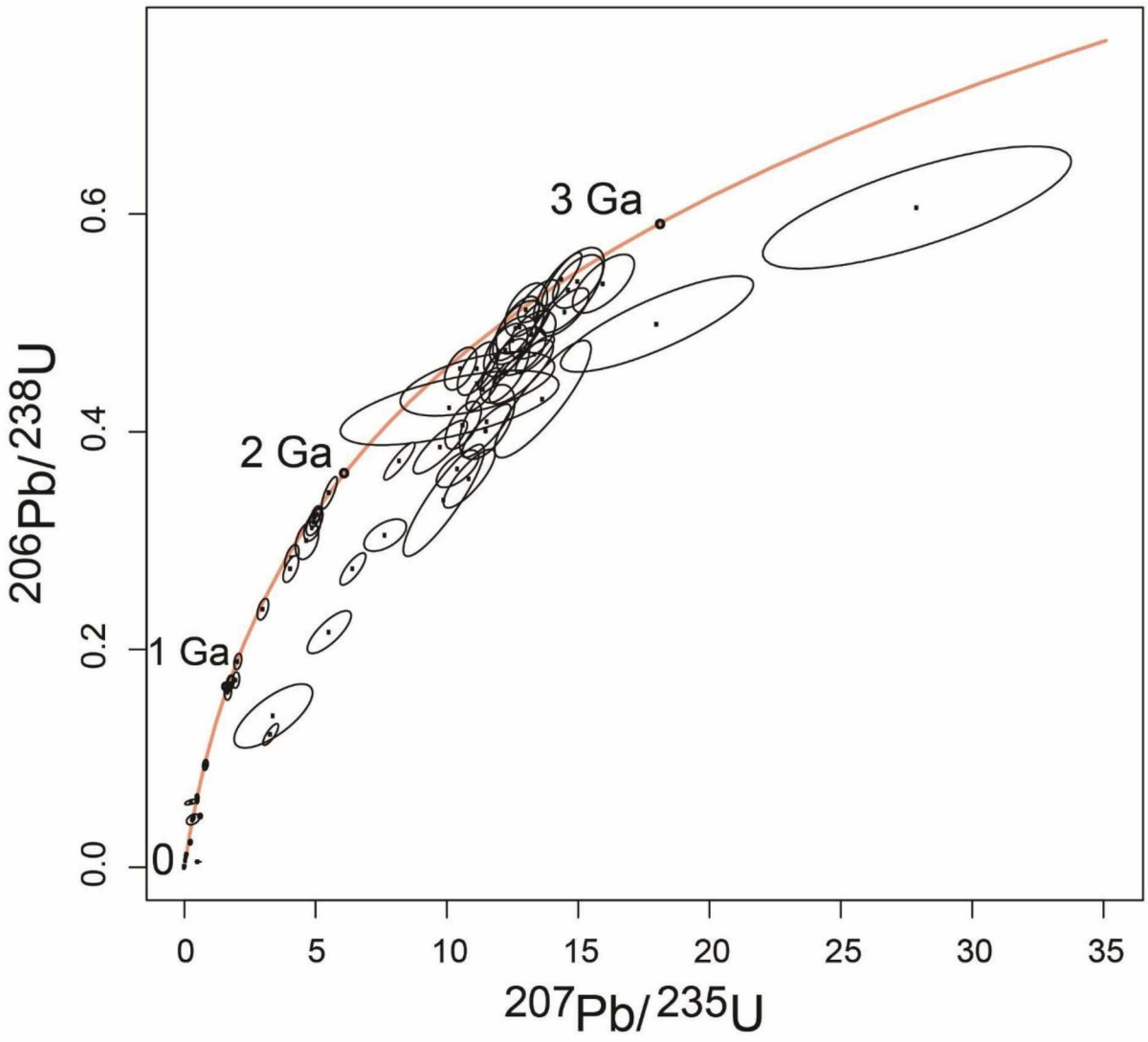

Figure A.1: Concordia plot of sample 16Ba03 that shows the large spread of U-Pb ages. Ages younger than ~70 Ma are considered to be contamination from either the separation lab or the analytical lab. Error ellipses are 2σ.